Fluid flow and Al transport during quartz-kyanite vein formation, Unst, Shetland Islands, Scotland

Claire E. Bucholz

Advisor: Jay J. Ague
Second Reader: Danny M. Rye
April 29, 2009

ABSTRACT

Quartz-kyanite veins, adjacent alteration selvages, and surrounding 'precursor' wall rocks in the Saxa Vord Pelites of Unst in the Shetland Islands (Scotland) were investigated to constrain the geochemical alteration associated with metamorphic fluid infiltration during the Caledonian Orogeny (~490-390 Ma). In particular, hypotheses concerning the mobility of Al, an element once thought to be mostly immobile during metamorphism, were tested. Samples of the vein, selvage, and precursors were collected, examined using the petrographic microscope and electron microprobe, and geochemically analyzed. Typical precursor mineral assemblages include various combinations of the index minerals chloritoid, staurolite, kyanite, and garnet all coexisting with quartz, muscovite, paragonite, margarite, and ±chlorite. The mineral assemblage of the selvages is the same regardless of metamorphic grade, consisting of chlorite, chloritoid, kyanite, quartz, muscovite, paragonite, and margarite. Pseudosections for bulk compositions of both selvage and precursors indicate that the observed mineral assemblages are stable at regional metamorphic conditions of ~550-600ºC and 0.8-1.1 GPa. Chemical compositions of the selvages and precursors were compared using a Zr reference frame to assess the characteristics and magnitude of geochemical alteration. Ti, Y, and REEs were added to the selvages due to growth of Fe-Ti oxides and monazite. Mass losses of Na, K, Ca, Rb, Sr, Cs, and volatiles were -50 to -60 % and resulted from the destruction of muscovite, paragonite, and margarite. Si was depleted from the selvages and transported to the veins. Al was residually enriched and in some cases added to the selvages, suggesting that the selvages were not the source of Al for the vein-kyanite and that Al was regionally, rather than locally, transported. The results of this study provide field evidence for Al mass transport at greenschist to amphibolite facies metamorphic conditions, possibly as a result of the elevated concentrations

of Al in metamorphic fluids due to alkali-Al silicate complexing at high pressures. Veins an order of magnitude thicker than those observed in the field are necessary to accommodate the Na and K lost from the selvages during alteration. Therefore, regional transport of Na and K out of the local rock system is inferred. In addition, to account for the observed abundances of kyanite and Fe-Ti oxides in the veins, large time-integrated fluid fluxes ($\sim 10^5$-10^6 m^3_{fluid}/m^2_{rock}) and fluid-rock ratios (10^2-10^3 m^3_{fluid}/m^3_{rock}) are required due to the small concentrations of Al and limited solubility of rutile in aqueous fluids. It is concluded that the quartz veins and the selvages were produced by large-scale advective mass transfer by means of focused fluid flow along an ancient thrust fault.

INTRODUCTION

Aluminum is the third most abundant element in the crust, yet its geochemical behavior in the deep crust during orogenic events is not fully understood. Aluminous minerals such as boehmite, corundum, and the Al_2SiO_5 polymorphs have traditionally been considered to have extremely low solubilities in deep crustal fluids based on both textural observations (e.g., Carmichael, 1969) and mineral-H_2O experiments (e.g., Anderson and Burnham, 1967; Burnham et al., 1973; Ragnarsdottir & Walther, 1985; Walther, 1997). However, the presence of Al-rich minerals including the Al_2SiO_5 polymorphs in veins and altered rock adjacent to veins indicates Al mobility during metamorphism (see Kerrick, 1990 for a review; Ague, 1995; Whitney & Dilek, 2000; Widmer and Thompson, 2001; Putlitz et al., 2002; McLelland et al., 2002; Sepahi et al., 2004; Beitter et al., 2008). Furthermore, recent experimental data has shown that Al transfer may occur in response to fluid-mineral equilibration under evolving metamorphic conditions (Verlaguet et al., 2006) and that Al-Si-Na complexing facilitates a significant increase in dissolved Al as Si and Na increase in solution (Manning, 2006; 2007;

3

Trooper & Manning, 2007; Newton & Manning, 2008). Elevated levels of Si in deep-crustal, high pressure settings would allow for considerable Al concentrations in fluids and increased transport of Al, yielding a plausible explanation for the occurrence of Al_2SiO_5 polymorphs in and around veins in contact and regional metamorphic rocks (cf. Manning, 2007).

Veins or mineralized fractures are clear indicators of mass transfer in regionally metamorphosed rocks, yet the nature and scale of mass transfer varies with the vein forming processes and the conditions of vein formation. The mass precipitated in veins is derived from the fluid flowing through a fracture, the surrounding wall rocks, or a combination of the two (Walther and Orville, 1982; Ferry and Dipple, 1992; Ague, 1994b; Widmer & Thompson, 2001; Philpotts & Ague, 2009). Field studies of quartz-kyanite veins have reached differing conclusions about the scale of Al mobility. Some studies infer regional transfer of Al, associating Al mobility with large channelized fluid fluxes (Ague, 2003a) or typical regional fluxes due to the devolitalization of sediments (Beitter et al., 2008), while other studies provide evidence for local derivation of Al (Widmer and Thompson, 2001). The nature and amount of transfer likely depends of the *P-T* conditions of metamorphism as well as the lithologies of the rock units involved.

The highly aluminous Saxa Vord Pelites in the northeast corner of the Island of Unst in the Shetlands (Scotland) contain numerous syn-metamorphic quartz-kyanite veins and are ideal for the study of fluid flow and mass transfer of Al and other elements. These veins are particularly notable for the presence of large splays of kyanite, as described in the classic paper of Read (1932). Furthermore, the veins in these rocks are surrounded by chemically and mineralogical altered host rock ('selvages'), indicating significant mass transfer between infiltrating fluids and the wall rocks. This study addresses the chemical and mineralogical

changes associated with vein and selvage formation, the length scales of fluid flow and element mass transfer, possible fluid sources contributing to vein formation, and the implications for Al mobility in deep crustal, orogenic environments. A fundamental objective is to test whether the Al that formed the vein-kyanite was transported regionally by fluids, or if it was derived more locally from adjacent wall rocks.

GEOLOGIC BACKGROUND

The Shetland Islands are located north of Mainland Scotland at approximately 60ºN and 1ºW (Fig. 1). Unst is the northernmost island and consists largely of basement rocks overthrust by an ophiolite complex. Obduction of the ophiolite complex began at ~500 Ma (498 ± 2 Ma; Flinn & Oglethorpe, 2005), during the onset of the subduction during the Grampian phase of the Caledonian Orogeny, or the collision of Baltica and Laurentia during the closure of the Iapetus Ocean (Flinn, 2007). Though this obduction age is slightly older than those for the ophiolite obduction dates in mainland Scotland and Ireland, it is equivalent to the dates of Norwegian ophiolites across the North Sea obducted onto the edge of Baltica (Dunning & Pedersen, 1988). The later Scandian Event (425-395 Ma) correlated with the final closure of the Iapetus Ocean is characterized by granitic magmatism and continued nappe thrusting on Unst (Flinn & Oglethorpe, 2005; Flinn, 2007). Garson & Plant (1973) suggested that this collisional boundary is analogous to the Highland Boundary Fault of the Scottish Mainland.

The rocks of northern Unst can be broadly divided into four major geological units: the Valla Field Block, the Shetland Ophiolite Complex, the Skaw Granite, and the Saxa Vord Block. The western half of northern Unst consists of the Valla Field Block, an extensively migmatized group of rocks predominantly of sedimentary origin. They are intruded by multiple sills, sheets of granite and granitic pegmatites, and dikes and sills of spessartite (Mykura et al.,

5

1976). The eastern side of Unst is composed of a nappe pile comprising various tectonic blocks of metamorphosed igneous and sedimentary protoliths. These blocks are part of the Shetland Ophiolite Complex, which was obducted during the Caledonian Orogeny (Flinn & Oglethorpe, 2005). The mafic rocks of the ophiolite complex, also known as the Main Serpentine and Greenstone Block, include peridotite-serpentinite, dunite-serpentinite, pyroxenite, and metagabbro or 'greenstone' separated by thrusts. Along the thrusts the rocks are altered to antigorite-serpentinite and talc, the latter of which is commercially mined in the area (Mykura et al., 1976).

The Skaw Granite crops out in the far NE corner of Unst (Fig. 1). It is an augen-granite with rectangular phenocrysts of potassic feldspar reaching 5 cm in length set in a highly-foliated matrix of quartz, muscovite, and biotite. Xenoliths of metasediment are commonly present. Flinn & Oglethorpe (2005) obtained an Ar/Ar cooling age of 425 ± 2.6 Ma from muscovite in the Skaw Granite. They suggest that the Skaw Granite and rocks of the upper section of the ophiolitic nappe were emplaced during a westward thrusting event associated with the onset of the Scandian Orogeny.

The Saxa Vord Block is separated from the Valla Field Block to the West and the Main Serpentine and Greenstone Block to the east by major shear zones. The Saxa Vord Block is composed predominantly of two units. One is the Queyhouse Flags, dominated by quartzofeldspathic and micaceous schists. The other is the Saxa Vord Pelites, micaceous, chloritic schists that, at appropriate metamorphic grade, contain chloritoid, staurolite, garnet, and kyanite or a combination thereof. The East Summit Pelite is a lithological subset of the Saxa Vord Pelites that is particularly garnet-rich. Also associated with the Saxa Vord Pelites are the Hevda Phyllites (chloritoid-free metapelitic phyllites) to the east (Fig. 1). The veins of this

study are found exclusively in the Saxa Vord Pelites and appear to be spatially associated with a regional thrust fault (the Hevda Thrust). The field relationships of the metapelitic schist precursors, the alteration selvages adjacent to the veins, and the quartz-kyanite veins are schematically shown in Figure 2.

The Saxa Vord Pelites have been interpreted as the northern continuation of the Dunrossness Phyllites of Mainland Shetland (Flinn et al., 1996). The Saxa Vord Pelites are similar to the Dunrossness Phyllites in that they are chloritoid-bearing and have a high Al content. They differ, however, in that the Saxa Vord Pelites were metamorphosed at greater pressures (Flinn et al., 1996).

Metamorphism

The Saxa Vord Pelites are strongly foliated, highly aluminous schists. Read (1934) and later Snelling (1957, 1958), Key (1972), Mykura (1976), and Flinn et al. (1996) recognized that the rocks underwent multiple phases of metamorphism. An early phase produced porphyroblasts that were subsequently pseudomorphed by white mica together with various combinations of chloritoid, kyanite, and/or garnet (Fig. 3a & b). These pseudomorphs are widely distributed across the field area. Relics of the original minerals are rare in the pseudomorphs. Relic staurolite has been found, and Flinn et al. (1996) infer other minerals including andalusite. In addition, we have observed ovoid pseudomorphs that may have originally been cordierite (Fig. 3b). This pseudomorph evidence suggests an early phase of relatively low-P, but high-T metamorphism. A later phase of metamorphism produced a series of index minerals generally indicative of a northerly increase in grade; key index minerals are chloritoid, staurolite, and garnet (Fig. 1). Kyanite is widespread, except at the very lowest grades in the southernmost part of the field area. Some rocks were affected by subsequent

retrogression which produced partial to complete chloritization of the staurolite, garnet, and chloritoid, replacement of staurolite by chloritoid, and sercitization of kyanite (e.g., Mykura, 1976; Flinn et al., 1996). Flinn et al. (1996) also report retrograde white mica-rich "shimmer aggregate" pseudomorphs after sillimanite near the contact with the Skaw Granite.

Flinn et al. (1996) concluded that an early phase of regional metamorphism produced the porphyroblasts that were later pseudomorphed. This phase was followed by contact metamorphism due to the intrusion of the Skaw Granite. These authors infer that the widespread chloritoid, kyanite, and staurolite in the Saxa Vord Pelites formed as part of a contact aureole around the granite. However, there is no clear spatial relationship between the Skaw Granite and the index mineral zones in the Saxa Vord Pelites, other than the thin band of shimmer aggregate pseudomorphs along the contact. We consider it more probable that a phase of relatively low-P, high-T metamorphism was followed by a much higher-P phase of regional metamorphism that gave rise to the observed distribution of index mineral zones. We discuss P-T conditions of metamorphism more fully using pseudosections, below. Clearly, major questions remain about the heat sources and the relative and absolute timing of metamorphic events in the area. We emphasize, however, that our study of fluid-driven mass transfer is independent of these questions.

METHODS OF INVESTIGATION

Macroscopic observations of little altered metapelitic schists, veins, and alteration selvages were made in the field. Samples were collected from localities chosen on the basis of freshness and proximity to geological features or units of interest. The widths of veins and their associated selvages were measured perpendicular to vein-wallrock contacts both in the field and on cut rock slabs.

Thin sections were examined optically and with the JEOL JXA-8600 election microprobe in the Department of Geology and Geophysics at Yale University. Semi-quantitative energy-dispersive spectrometer (EDS) analyses were collected to constrain Fe-Ti oxide mineral compositions.

The samples were broadly categorized as precursor host rock far-removed from vein alteration, vein selvage, or quartz-kyanite vein. These were prepared for chemical analysis by isolating the sample portion of interest using a rock saw. The cut surfaces were abraded with carbide paper to remove any contamination due to sawing. The samples were then ultrasonically cleaned in distilled, deionized water. 13 precursor, 22 selvage, and 3 quartz-kyanite vein samples were ultimately selected based on their freshness and suitability for chemical analysis. Chemical analyses for major and trace elements were done by SGS Minerals Services using X-ray fluorescence (XRF) and inductively coupled plasma-mass spectrometer (ICP-MS) techniques (Tables 1 & 2; see Ague, 2003a, for a summary of analytical methods).

Pseudosections were constructed for representative bulk compositions of the precursor schists as well as the altered selvages in order to constrain the pressure and temperature regime of metamorphism and fluid infiltration. This was done using version 15.05.08 of the Theriak/Domino software of Christian de Capitani and Konstantin Petrakakis (http://titan.minpet.unibas.ch/minpet/theriak/theruser.html). The Domino program calculates equilibrium assemblage phase diagrams using Gibbs free energy minimization. The thermodynamic data was taken mostly from the internally consistent database supplied with the program. However, we adjusted the standard enthalpy of formation of Mg-staurolite in order to match, as closely as possible, the staurolite stability field of Powell et al. (1998) for typical Fe-

rich metapelitic bulk compositions. The enthalpy used was -25072.594 kJ mol^{-1}, and the entropy, molar volume, and heat capacity were from Holland and Powell (1998).

RESULTS

Mineral Assemblages and Petrography

Metapelitic Schist Precursors

Metamorphic grade in the Saxa Vord Pelites generally increases to the north. In the south-southwest, the rocks are composed mostly of white mica (muscovite+paragonite±margarite), quartz, chloritoid (Cld), and chlorite (Chl). At this and higher metamorphic grades, Fe-Ti oxides (±rutile±ilmenite-hematite±magnetite) are widespread. Kyanite (Ky) is also found, particularly in and around quartz veins. Garnet (Grt) is rare, but mineral assemblages of white mica+quartz+Cld+Grt±Chl are locally present. With increasing grade, staurolite (St) appears, chloritoid and chlorite are less abundant, and garnet remains rare. Typical mineral assemblages are: St+Cld±Chl, Cld+Ky, and St+Cld+Ky (all coexist with white mica and quartz). At the highest grades, garnet becomes more abundant and there is considerable diversity in the mineral assemblages. Common assemblages include: Grt+St+Chl, Grt+St+Ky+Chl, and Grt+St+Cld±Chl (all coexist with white mica and quartz).

Selvages

Selvages around veins are generally <15 cm in thickness and are composed predominantly of chloritoid, kyanite, chlorite, Fe-Ti oxides, and white mica. The selvage rocks are distinctly coarser grained than the precursor schists, and contain less white mica and quartz, but more kyanite, chlorioid, and Fe-Ti oxides. The original metamorphic fabric is preserved in a few of the selvages, but it is usually destroyed due to the growth of new minerals. The Fe-Ti

oxides are present in wormy bands of individual euhedral crystals and are commonly associated with chlorite (Fig. 3c).

Veins

The Saxa Vord Pelites bear extensive evidence of massive quartz veining. The veins range in width from several millimeters to the meter scale; most are a few centimeters to a few decimeters wide. Field observations indicate that outcrops contain a few percent to as much as ~20 volume percent quartz veins. Quartz is the primary mineral in the veins. In thin section, it generally displays prominent undulose extinction. Accessory minerals include kyanite, hematite-ilmenite solid solution oxides, rutile, chlorite, apatite, and monazite (Fig. 3d-f). Kyanite is present as large radiating splays of elongate crystals that can measure up to 5 cm long. Oxides are not common; where present they are found as elongated, slightly curved crystals or masses of crystals as much as several cm long. Blades of kyanite and, in some rocks, large Fe-Ti oxide grains may be bent and/or fractured. In a few samples, hematite-ilmenite solid solutions grew around earlier formed and fractured rutile (Fig. 3d). Large (~200 μm) apatite crystals in or adjacent to veins are fractured and have monazite growing within the cracks (Fig. 3e).

Pseudosection Analysis

Pseudosections were constructed to assess the *P-T* regime of metamorphism and vein formation. Calculations were done for the system $Na_2O-K_2O-FeO-MgO-Al_2O_3-SiO_2-H_2O$ (NKFMASH). Although traces of margarite are reported in some rocks (Flinn et al., 1996), CaO was neglected as it is a minor constituent.

Precursor Pseudosection

Two pseudosections for the bulk composition of the representative precursor sample

JAB165A2 were calculated to investigate the impact of variations in Fe^{2+}-Fe^{3+} content on

mineral assemblages (Fig. 4a, b). The first pseudosection takes all of the Fe from the XRF

analysis to be in the 2+ oxidation state, whereas the second uses 75 mole % Fe^{2+} and 25 mole %

Fe^{3+}. The first pseudosection is intended to represent metapelites that were hematite-ilmenite-

and magnetite-poor, whereas the second represents rocks containing greater amounts of oxides.

Of course, a wide range of other ferrous/ferric ratios are possible; however, the values used

illustrate in a general way how stability fields would be expected to change with composition.

Using the peak mineral assemblages progressing northward through the Saxa Vord

Pelites, a metamorphic field *P-T* gradient was constructed. The lowest grade assemblages

contain muscovite, paragonite, chlorite, chloritoid, and quartz. At higher metamorphic grades,

the destruction of chloritoid typically produced staurolite. In some rocks poor in oxides,

assemblages containing Grt+Cld±Chl grew. At the highest grades, muscovite, paragonite, and

quartz are found together with amphibolite facies mineral assemblages including Grt+St+Chl,

Grt+St+Ky+Chl, and Grt+St+Cld±Chl. These assemblages are stable in and around the AFM

invariant point assemblage Grt+St+Cld+Ky+Chl at about 605ºC and 1.15 GPa (Fig. 4). These

conditions are very similar to those calculated in other studies, such as Powell et al. (1998). In

fact, our petrographic observations indicate that the AFM invariant assemblage

Grt+St+Ky+Cld+Chl may even have formed, although the textural interpretation of the relative

timing of chlorite formation, whether prograde or retrograde, is somewhat ambiguous. We

conclude that the peak conditions were reached near the invariant point at high pressures.

Overall, the progression of mineral assemblages defines a metamorphic field *P-T* gradient in

the temperature range of 550-600 ºC and a pressure range of 0.8-1.1 GPa. This *P-T* range is in

agreement with other studies of quartz-kyanite veins (e.g., Ague, 1995) and is indicative of crustal depths of 25-35 km during peak metamorphism.

The biotite stability field is shown as an upper temperature limit as biotite is not found. The cordierite stability field is located at lower pressures. The absence of cordierite from amphibolite facies Saxa Vord Pelites indicates that regional metamorphic pressures were in excess of ~0.5-0.6 GPa. If some of the pseudomorphs were originally cordierite, the early phase of metamorphism took place at or below these pressures.

Selvage Pseudosection

A pseudosection for the bulk composition for representative selvage sample JAB181Aiii was also calculated (Figure 5). The selvages generally have an increased amount of Fe-Ti oxides relative to the precursor schists. Using the modal amount of hematite-ilmenite solid solution together with the approximate mole percentage of hematite and ilmenite from EDS analysis, the appropriate amount of ferric iron associated with hematite-ilmenite solid solutions was then calculated and subtracted from the total iron. The resulting value was assumed to be the amount of ferrous iron in the sample. The pseudosection was calculated using only ferrous iron, which is reasonable considering that chloritoid, the primary iron-bearing silicate mineral in the selvages, is dominated by Fe^{2+}.

Across all metamorphic grades the selvages contain chloritoid, kyanite, muscovite, paragonite, chlorite, and quartz. This mineral assemblage defines a large stability field bounded at high temperatures by the assemblages Chl+St+Ky and Chl+Grt+Ky (Fig. 5). Garnet and staurolite are not observed in the selvages. The selvages contain considerably less K and Na and more Al than precursor schists far-removed from veins. These chemical relationships expand the stability field for the highly aluminous assemblage Chl+Cld+Ky in selvages relative

to precursor schists. The range of prograde *P-T* conditions inferred from the precursors falls within the Chl+Cld+Ky stability field calculated for the selvages.

Mass Transfer Relationships

The mobility of "non-volatile" rock-forming elements associated with regional metamorphic fluid flow has been demonstrated by several studies through the examination of metamorphic veins and their associated alteration selvages (e.g., Ague, 1994a; b; Oliver et al., 1998; Masters and Ague, 2005; Penniston-Dorland and Ferry, 2008). Although studies that quantitatively assess vein-selvage systems are highly useful, an insufficient number have been undertaken to constrain the general nature, degree, and spatial scale of element mobility and fluid infiltration during different grades or styles of metamorphism. By quantitatively addressing the mass changes between the precursor and selvage rocks using the relationships outline below, this study specifically addresses the following questions: (1) was their significant mass transfer of elements other than Si in the formation of the veins and selvages; (2) was the mass transfer at a local or regional scale; (3) what magnitude of fluid flux was necessary to form the veins and associated alteration selvages?

Defining a Geochemical Reference Frame

In order to quantitatively assess mass gains or losses of elements in the selvages, an immobile reference element or group of elements must be chosen. This reference element is taken to be relatively immobile during the alteration of the selvage. Although no element is completely immobile, some have exceedingly low concentrations in solutions and may be used satisfactorily as reference elements. Commonly, high field strength elements such as Zr, Ti, Th, and the rare earth elements (REE) are used (Ague, 2003a; Penniston-Dorland and Ferry, 2008).

Yet, each of these elements may be mobile under certain pressures, temperatures, and fluid compositions and must therefore be assessed for immobility (e.g., Bröcker and Enders, 2001).

Ubiquitous monazite growing in cracks of fractured apatite grains in and around veins eliminated the REEs as potential reference elements (Fig. 3f). Furthermore, large crystals of ilmenite-hematite solid solutions and rutile growing within the veins as well as widespread Fe-Ti oxides in many of the selvage rocks suggested that Ti was mobile as well (Fig. 3d). Zr is predominantly hosted by zircon, which has an extremely low solubility in typical metamorphic fluids (Ayers and Watson, 1991; Carlson, 2002). Zr morphologies varied little across selvage traverses and microprobe reconnaissance demonstrated that zircons were absent from vein samples, suggesting that Zr was neither added to nor loss from the selvage during fluid infiltration. For these reasons, Zr was chosen as the reference to assess mass gains and losses. Nb, Hf, Th, and Cr also typically have small concentrations in metamorphic fluids; as shown below, their geochemical behavior was identical, within error, to that of zirconium (Fig. 6).

Basic Equations

The following equations for the changes in rock mass follow Ague (1994a), Ague and van Haren (1996), and Philpotts and Ague (2009) and references cited therein.

$$T_{mass,i} = \frac{c_i^0}{c_i'} - 1 \quad (1)$$

$T_{mass,i}$ is the total rock mass change calculated using immobile reference species i. $T_{mass,i}$ is a fraction and the percentage mass change can be found by multiplying it by 100. The superscripts 0 and ´ indicate the precursor and altered rocks, respectively. If rock mass has been lost, then the concentration of i will be greater in the altered rock than in the precursor rock.

Conversely, if rock mass has been gained, then the concentration of i will be less in the altered rock than it the precursor rock.

The mass change of a mobile species j is:

$$\tau_i^j = \left(\frac{c_i^0}{c_i'}\right)\left(\frac{c_j'}{c_j^0}\right) - 1 \quad (2)$$

where c_j indicates the concentration of j and τ_i^j is the fractional mass change for j. Uncertainties were estimated following Ague (1994a) and Philpotts and Ague (2009).

Analysis of Mass Transfer

Mass Percent Change Diagram

The mass transfer involved in the formation of the vein selvages was evaluated graphically by plotting the mass percent changes and uncertainties of specific elements of interest (Fig. 6). These values represent the average chemical alteration that produced the selvages from the precursor schists during vein formation. On average, the selvages lost Si, Na, K, Rb, Ca, Sr, Ba, Cs, and volatiles, and gained Y, REE, and Ti. The losses of Na, K, Rb, Cs, Ba, and Sr were very large, ranging from about -50 % to more than -60 %. Si underwent similar large mass changes near -50 %. Average gains of REEs were considerable, varying from 115 to 130 % for the LREEs and 40 to 130 % for the HREEs. Gains of Y in excess of 100 % are also indicated. Although the mass changes for Al and Fe are not statistically significant, mass gains are suggested.

Wedge Diagrams

The mass percent change diagram depicts the average mass changes of individual elements in the selvages, but it does not show variation of individual samples among a

population. Wedge diagrams are a simple graphical technique that allows for individual samples to be examined in addition to revealing the broader style of geochemical alteration that produced the observed mass changes. Plotting the concentration of a mobile element j versus a reference element i for precursor samples will yield a cloud of points because the protoliths in the original sedimentary section were compositionally heterogeneous. The outer edges of this cloud will define a wedge-shaped region that converges on the origin. This wedge can be used as a reference frame to determine whether an element was gained, loss, residually enriched, or residually diluted from a suite of samples (Fig. 7; Ague, 1994a; Philpotts and Ague, 2009). Residual enrichment refers to an increase in concentration of the element of interest due to overall rock mass loss, whereas residual dilution is a decrease in concentration due to overall rock mass gain. If the concentrations of selvage samples are plotted, they will lie outside of the reference frame wedge and facilitate the identification of mass changes or a residual enrichment or dilution of j.

Wedge diagrams for the key constituents Si, Al, Na, K, LOI (loss on ignition—a proxy for volatiles), and Y are shown in Figure 7. Although some scatter in the data is evident, there is little doubt that in general Si, Na, K, and volatiles were lost from the selvages. The Si-Zr systematics of two samples, however, indicate that they gained Si (Fig. 7a). The loss of volatiles is consistent with prograde dehydration of the rocks during selvage formation (Fig. 7e). The elevated volatile contents of a few of the samples are inferred to be the result of limited retrograde hydration. Al appears to have been initially residually enriched and then subsequently added to some of the selvages (Fig. 7b). The residual enrichment of Al was largely the result of Si loss from the selvages. Therefore, the addition of Al to some of the

selvages probably took place after most of Si had been lost. Y was also added to the selvages (Fig. 7f).

Geochemical Traverses

During metamorphic fluid infiltration rocks adjacent to veins will change composition in order to eliminate chemical potential gradients that arise due to the juxtaposition of a compositionally distinct fluid phase. Geochemical traverses perpendicular to vein-selvage contacts yield insight into the magnitude and length scale of this metasomatic alteration. Two geochemical traverses from sample sites 181 and 186A were taken perpendicularly across selvage-vein contacts (Fig. 8). The thicknesses of the veins adjacent to the 181 and 186A traverses were approximately 30 and 10 cm, respectively.

In both geochemical traverses, Si is depleted in the selvage wall rock (Fig. 8a). The traverses did not span the entire depletion zone for Si as the most distal values are still well below those of the average precursor rock. Noticeably, the Si/Zr ratios for the samples adjacent to the vein, in particular 181Aii, are larger than that for the more distal samples in the traverse. Small quartz veinlets penetrate up to ~6 cm of the selvage bordering the vein and were partially incorporated into samples 181Aii-iv, explaining the larger Si/Zr values.

Alkalis (Na, K, Rb) and alkaline earths (Sr, Ba) are depleted from in the selvages (Fig. 8c-g). The most distal samples from the vein in traverse 186A have ratios similar to those of the precursors, indicating that the 186 traverse extends across the entire zone of depletion for these elements. In contrast, the ratios for the 181 traverse do not regain precursor values, indicating that the 181 traverse does not extend across the entire width of alteration. For the 181 traverse, the Na/Zr, K/Zr, Rb/Zr, and Ba/Zr values directly at the margin of the vein are larger than for the other samples in the traverse due to minor scericitization of kyanite in the selvage closest to

the vein. This, however, is a retrograde reaction that occurred after the main episode of vein formation and selvage alteration. In spite of retrogression, ratios for 181Aii are still significantly smaller than the lowermost 2 sigma sample standard deviation bounds (Fig. 8c-f).

Y and LREEs were added directly adjacent to the vein, whereas HREEs show substantial, but not as pronounced addition (Fig. 8f, g). Sr/Y ratios are uniformly low and decrease towards the vein due to the addition of Y and loss of Sr in the selvages. In general, the REEs demonstrate variable mass addition with some selvages indicating addition and others not. This variability explains the large error bounds of the REEs on the mass percent change diagram (Fig. 6).

In the 181A traverse, Al/Zr ratios increase towards the vein, indicating Al addition due to vein-induced alteration (Fig. 8b). Small quartz veinlets adjacent to the vein margin contained kyanite, explaining the larger Al/Zr ratios for the samples most proximal to the vein. No significant changes in the Al/Zr ratio are evident for the 186A traverse. Al addition was variable throughout the population of selvages; both residual enrichment and residual enrichment with subsequent mass gains are observed. From the wedge diagrams it appears that residual enrichment without subsequent mass addition was more common.

Noticeably, the length scales of alteration for the 181 and 186A traverses and for the various elements are different. For example, Si is highly mobile and has the longest length scale of alteration, not attaining precursor values over the extent of both the traverses. Si/Zr ratios for the 181 traverse are larger proximal to the vein due to the penetration of small quartz-kyanite veinlets. This "veinlet effect," however, does not obscure the overall trend of silica depletion from the selvages. Al/Zr ratios adjacent to the vein in the 181 traverse are also elevated due to the "veinlet effect." Both the more distal samples for the 181 traverse as well as the all the

samples in the 186A traverse exhibit precursor Al/Zr ratios, suggesting a short length scale of alteration for Al. Alkali and alkaline earth Zr-ratios attain precursor values at 8-10 cm for traverse 186A, but are still well below precursor values in traverse 181 at 14 cm. The La length scales are considerably smaller, on the order of ~5 cm for the 181 traverse, indicating lesser degrees of mobility for REEs within the selvage. The difference between the length scales of the two traverses is likely a result of the thickness of the individual veins. The vein-selvage relationships of this study and those of others (e.g., Ague, 1994b) indicate that the ratio of the total width of the selvage (the sum of the selvage widths on either side of the vein) and the width of the vein varies between 1:1 and 2:1. Therefore, larger veins are expected to have larger selvage widths. The vein adjacent to the 181 traverse was ~30 cm thick, while that of the 186A traverse was only ~10 cm thick. As expected, the selvage and thus length scale of alteration around the 181 vein is greater than that of the 186A vein.

DISCUSSION

Timing of Vein and Selvage Formation

The chronological relationship between vein formation and metamorphism is important to establish. Vein formation and peak metamorphic conditions have been shown to be contemporaneous in other regional geological settings, such as the Barrovian garnet zone of Mainland Scotland (e.g., Breeding et al., 2004). Initial lithological examination and pseudosection analysis suggests that this is the case for the Saxa Vord Pelites. The coarse-grained texture of the selvages is suggestive of a fluid rich, metamorphic environment of formation. In addition, the selvages lost volatiles, indicating that vein formation was contemporaneous with prograde metamorphic devolatization reactions. Furthermore, the stability field of Chl+Cld+Ky on the selvage pseudosection lies within the metamorphic field *P-*

T gradient that was defined for the precursor pseudosection (Figs. 4 & 5). The peak

metamorphic mineral assemblages and the selvage mineral assemblage are stable at similar *P-T*

conditions and, thus, the veins and selvages could have formed at or near peak metamorphic

conditions. The above observations, however, do not preclude some degree of veining during

exhumation given the broad stability field of the selvage mineral assemblage.

Mineralogical Changes and Mobility of Elements

The formation of selvages around the veins of the Saxa Vord Pelites involved

significant mass transfer of certain non-volatile elements. This section examines the

mineralogical changes associated with the geochemical alteration.

Silica

The majority of selvage samples were depleted in Si, but a few samples indicate Si gain

from the wedge diagrams (Fig. 7a). These relationships suggest that although Si was generally

depleted from the selvage, there was also Si transport and precipitation by through-going fluids.

The Si removed from the selvages could have then been deposited in adjacent fractures or

transported out of the system through channelized fluid transport.

Alkalis and Alkaline Earths

Na, K, Rb, Sr, Ba, Ca, and Cs were all lost during the destruction of muscovite,

paragonite, and margarite in the host rock. These elements have been shown to be mobile in

metamorphic vein systems in other field studies (e.g., Ague, 1994a,b; Oliver et al., 1998; Ague,

2003a; Masters and Ague, 2005; Penniston-Dorland & Ferry, 2008). For example, Na gain with

contemporaneous K loss due to growth of albite and destruction of muscovite has been

demonstrated for other vein-selvage systems (Ague, 2003a; Breeding and Ague, 2002).

However, the simple exchange of cations like Na (±Ca) for K cannot explain the geochemical alteration of the selvages of this study. Rather a loss of both alkalis and alkaline earths is documented. The fluids responsible for depleting these elements from the host rocks must have been undersaturated in these elements, preferentially stripping Na and K from the rock during infiltration.

Yttrium and REEs

Though conventional literature (c.f., Bau, 1991) has argued for the limited mobility of REEs in metamorphic fluids, this study and others indicate that REEs may be highly mobile in metamorphic and hydrothermal fluids (e.g., Pan and Fleet, 1996; Bau and Dulski, 1995; Whitney and Olmsted, 1998; Boulvais et al., 2000; Ague, 2003a). Gains of Y, Ce, and other light REEs in the selvages are explained by the formation of monazite around apatite grains (Fig. 3f). P appears to have been locally mobile, added to some selvages and lost from others to form apatite in and around veins, but does not display the same mass transfer patterns as Y or REE and therefore was not likely involved in the transport of these elements. It has been suggested that CO_2- and halogen-rich fluids are capable of transporting REEs by means of fluoride, chloride, and carbonate complexing with REEs (Gieré and Williams, 1992; Bau and Dulski, 1995; Pan and Fleet, 1996). However, there is not evidence for significant CO_2 or halogen components in the fluids that formed the veins of this study. Rather, the association of REE addition with Y addition indicates that REEs may have been transported by Y complexes and then sequestered into monazite (Ague, 2003a). Further discussion on this topic awaits experimental work pertaining to REE mobility in metamorphic fluids.

Titanium

Ti and possibly Fe appear to be residually enriched or gained during the formation of Fe-Ti oxides in the selvages and large rutile in the veins. This observation suggests Fe-Ti regional mobility. Although Ti has traditionally been thought to have low solubility in aqueous fluids due to low concentrations in surface and diagenetic fluids (see van Baalen, 1993 for review) and experimental studies indicating low rutile solubility at moderate P and T (Schuiling and Vink, 1967; Agapova et al., 1989), rutile may demonstrate elevated solubility at appropriate conditions (van Baalen, 1993; Jiang et al., 2005). In particular, exhumed high-P metamorphic rocks contain evidence for elevated rutile solubility, such as rutile in veins (e.g., Selverstone et al., 1992; Franz et al., 2001; Gao and Klemd, 2001; Rubatto and Hermann, 2003; Gao et al., 2007), Ti-bearing minerals in fluid inclusions (e.g., Philippot and Selverstone, 1991), and alteration in whole-rock TiO_2 concentration (e.g., Sorensen and Grossman, 1989; Bröcker and Enders, 2001; Gao et al., 2007). Furthermore, a recent experimental study has demonstrated that Ti-complexing with dissolved Na-Al silicates in a H_2O-rich fluid phase at mid- to deep-crustal settings can greatly enhance Ti solubility and trasnport (Antignano & Manning, 2008). The dissolved Si, Al, and Na present in the fluids that formed quartz veins during high-P metamorphism of the Saxa Vord Pelites would have facilitated complexing and Ti mobility during fluid-rock interaction.

Aluminum

Although the mass changes for Al are not statistically significant, the Al wedge diagram indicates that Al was residually enriched in all of the selvages (Fig. 7b). Silica loss from the selvages probably caused most of the residual enrichment of Al. Subsequently Al was added to some of the selvages, but not to all. One or two of the selvage samples indicate Al loss, which

could account for some local Al transport from the selvages to the veins, but larger-scale transport would have been necessary to form the large amounts of vein kyanite.

This study provides a field application for recent experimental work pertaining to Al solubility at elevated pressures and temperatures. Corundum solubility in pure H_2O increases with pressure, but the solubility at 800ºC and 1 GPa is still quite low at 1.3 mmolal (Tropper & Manning, 2007). For comparison, the solubility of quartz at equivalent conditions is three orders of magnitude greater (Manning, 1994). However, complexing with alkalis and/or halides (Diakonov et al., 1996; Tagirov and Schott, 2001; Walther, 2001; Newton and Manning, 2006) and with aqueous silica and/or alkalis (Salvi et al., 1998; Manning, 2007; Newton and Manning, 2008) have been shown to increase the concentration of Al in aqueous solutions at various *P-T* conditions. Indeed, experiments demonstrate that Al concentrations in Si-bearing solutions at 700ºC and 1.0 GPa may reach 5.80 ± 0.03 mmolal due to the formation of Al-Si complexes (Manning, 2007). Other experiments indicate that the simultaneous addition of NaCl and SiO_2 to fluids at 800ºC and 1.0 GPa leads to an even greater increase in Al concentrations than either component would produce alone due to Na-aluminosilicate polymerization (Newton and Manning, 2008). K-aluminosilicate polymerization is also likely. The fluids that deposited the veins on Unst were saturated in Si and contained dissolved Na and K as well. The enhanced solubility of Al-complexes at high pressures in Si- and alkali-bearing fluids could explain the abundant kyanite in the veins and the enrichment of Al in some of the selvages.

Possible Sources of Fluid

The fluid that formed the veins on Unst could be derived from one of several possible local source regions. The ultramafic ophiolite of Unst is an unlikely source for the fluids due to the lack of enrichment in Mg, Cr, or Ni in the selvages. The Skaw Granite is also not likely as it

is potassium-rich and would have released K-rich magmatic fluids that would have stabilized muscovite rather than destroy it in the selvages. The Queyhouse Flags, another local source, are muscovite-rich and plagioclase-bearing and are thus an unlikely source for fluids that would destroy muscovite in the chloritoid-schists. Though none of these potential fluid origins seems probable, one possibility is that the alteration front observed in the sampled selvages was far enough removed from the source for the fluid to have equilibrated with surrounding schist and did not produce ultramafic or potassic alteration. Yet, this is unlikely because of the close proximity of all these rock units to the Saxa Vord Pelites. For example, the contact with the Skaw Granite is at most 2-3 km away from the sample sites and sample JAB198, taken directly adjacent to the contact, does not appear to have any K- or Na- rich alteration. An alternative source could be the devolitization of the rock unit itself or deeper metapelitic rocks underlying the Saxa Vord Pelites. As the schists are cut by a large fault (Hevda Thrust; Fig. 1), the fluids produced from the dehydrating rocks could have been focused along conduits formed during fracturing events, which then became the sites of quartz-kyanite vein precipitation. Although the source of the fluids cannot be identified definitively, more deeply derived fluids with the appropriate chemical composition to produce the observed alterations in the selvages must have been channelized along the vein-rich zone.

Magnitude of Fluid Infiltration

Several methods were used to determine whether fluid flow was local or regional and to constrain what magnitude of fluid fluxes were required to produce the veins and selvages. First, it was evaluated whether the K and Na lost from the selvages could be accounted for by local redistribution to the vein. To do this, average K and Na contents of the veins were used to calculate the thickness of veins necessary to accommodate the K and Na lost from the selvages.

These values were then compared to the thicknesses of veins observed in the field. Average K_2O and Na_2O contents for two representative vein analyses of 0.085 and 0.13 weight %, respectively, were used. Calculated average mass losses for K_2O and Na_2O of 58.4% and 61.6%, respectively, equate to a mass loss of 1.65 wt. % K_2O and 1.01 wt. % Na_2O for an average precursor composition. Changes in the volume of the rock during selvage alteration must be accounted for in order to ascertain the original volume of rock altered and, therefore, the amount of K_2O and Na_2O lost. The volume strain using Zr as a reference element was calculated using the following equation (Ague, 1994a):

$$\varepsilon_i = \left(\frac{c_i^0}{c_i'}\right)\left(\frac{\rho^0}{\rho'}\right) - 1 \quad (3)$$

where c_i^0 is the average concentration of Zr in the precursor rocks and c_i' is the average concentration of Zr in the altered selvages. Representative precursor (ρ^0) and selvage (ρ') densities of 2.80 g/cm^3 and 2.90 g/cm^3, respectively, were calculated using the Theriak-Domino software. Using these values the resulting volume strain was -28.9%. For an average thickness of 10 cm for selvage on either side of a vein (20 cm total) the observed loss of K_2O and Na_2O and corresponding volume strain would require a vein ~580 cm and ~230 cm thick, respectively. Most veins observed in the field were a few tens of centimeters wide; a vein of meter-scale thickness was only observed once. Therefore, the above calculation requires veins an order of magnitude thicker, on average, than observed, suggesting considerable transport of these elements out of the rocks over the entire area via regional fluid flow.

Whereas Na-K mass balance calculations confirm non-local transport of mass, the actual magnitude of fluid infiltration may be addressed through the Al content of the veins. The

following expression describes advective mass transport under local fluid-rock equilibrium (Ague, 2003a):

$$q_{TI} \approx L\frac{M_e}{\Delta C_e} + L\phi \quad (4)$$

where q_{TI} is the time-integrated fluid flux, L is the characteristic distance of chemical alteration, M_e is the moles of e added (positive) or removed (negative) per volume rock, ΔC_e is the difference in the concentration of element e between the input and equilibrium fluids (i.e. the concentration drop in moles e per m^3 fluid), ϕ is the porosity. We assume that the porosity was relatively small and, thus, neglect the $L\phi$ term. The ratio $M_e/\Delta C_e$ is equivalent to the 'classic' fluid-rock ratio, or the volume of reactive fluid that interacted with a unit volume of rock (Bickle, 1992). Given that the porosity value is $\ll1$, any fluid-rock ratio in excess of 1 indicates significant fluid infiltration. A value of 4.09 x 10^{-3} mol Al/cm^3 vein was estimated for M_{Al} using a representative average vein composition from samples 175Ai and 181Ai of 7.87% Al_2O_3 and an approximate vein density of 2.65 g/cm^3. The value of ΔC_e was calculated for several values of typical Al concentrations between 10^{-2} to 10^{-3} m (Manning, 2007; Beitter et al. 2008), which were then converted to moles of Al per kg of solution assuming quartz saturation. The density of supercritical H_2O at 600ºC and 0.8 and 1 GPa was calculated as ~907 and ~955 kg/m^3, respectively, using the Redlich-Kwong equation of state from Kerrick and Jacobs (1981). The results of the calculations using the 1 GPa density value are shown in Table 3. Calculations using the 0.8 GPa density value yielded only slightly larger fluxes with the same orders of magnitude.

These calculations demonstrate that large fluid-rock ratios on the order of 10^2 to 10^3 were required for the observed Al concentration in the veins regardless of the value of L. The

cause of Al precipitation is unknown, but possibilities include variations in T, P, pH, and fluid composition (eg., Manning, 2006; 2007; Beitter et al., 2008). The fluid-rock ratio would be overestimated if Al was derived locally from the selvages. However, local derivation of Al for precipitation in the veins is not indicated from the Al-Zr wedge diagram and thus, local derivation is considered to not significantly affect the fluid-rock ratio values. Indeed, the regional distribution of veins on Unst indicate a probable value for L of 100-1000 m, suggesting that time-integrated fluid fluxes could have easily reached 10^5-10^6 m$^3_{fluid}$ /m$^2_{rock}$ (Eq. 4; Table 3; Fig. 9). This magnitude of fluid flux through individual veins is similar to that for veins found in other metamorphic settings, including the Wepawaug Schist, Connecticut ($\sim$3$\cdot$10^5 m$^3_{fluid}$ /m$^2_{rock}$; Ague, 1994), the Otago Schist, New Zealand ($\sim$5$\cdot$10^6 m$^3_{fluid}$ /m$^2_{rock}$; Breeding and Ague, 2002), and the Waits River Formation, Vermont ($\sim$4-9$\cdot$10^5 m$^3_{fluid}$ /m$^2_{rock}$; Penniston-Dorland and Ferry, 2008).

In addition to kyanite, the presence of rutile and Fe-Ti oxides in veins indicates Ti transport (Fig. 3d). Although controversy exists regarding the solubility systematics of rutile, Ti concentrations in aqueous fluids with or without dissolved Na-Al silicates are low, of the order of 10^{-4}-10^{-5} m at 1.0 GPa and 600ºC (Ayers & Watson, 1993; Antignano & Manning, 2008). Consequently, time-integrated fluid fluxes must have been large to transport significant quantities of Ti, consistent with the large fluxes estimated based on Al mass transfer.

Other recent studies have addressed the question of how much fluid is necessary to form systems of quartz-kyanite veins. Beitter et al. (2008) propose that the quartz-kyanite veins of the Alpe Sponda in Switzerland were formed by large volumetric fluid-rock ratios of $\sim$1,500. They argue that the vein mass was not locally-derived and thus must have been precipitated from migrating fluids. Ratios of $\sim$1500 are comparable to our estimates for the quartz-kyanite

veins of Unst (Table 3; Fig. 9). Importantly, Beitter et al. calculated their fluid-rock ratio using a somewhat different method than used here and, thus, the agreement between our two studies is encouraging. However, Beitter et al. (2008) conclude that large fluid fluxes were not necessary to precipitate the Alpe Sponda veins, and that typical regional metamorphic devolatilization would have been adequate.

The time-integrated fluid flux generated at the top of a 10 km thick metapelitic sequence will be of order 10^3 m^3 m^{-2} (see review in Ague, 2003b). This quantity is very different than the volumetric fluid-rock ratio (cf. Bickle, 1992). The volumetric fluid-rock ratio can be thought of as the volume of fluid that has reacted with the rock, not the total volume of fluid that has passed through the rock. As a result, such fluid-rock ratios are different for different elements or isotopic tracers, leading to considerable confusion in the literature. Conversely, the time-integrated fluid flux refers to the total amount of fluid that has passed through a rock over a unit area. As shown by Ferry and Dipple (1991), the q_{TI} values needed to precipitate quartz veins by fluid flow down typical temperature and pressure gradients are immense, of order 10^6 m$^3_{fluid}$ m$^{-2}_{rock}$ or larger. As a consequence, a typical regional devolatilization flux of 10^3 m$^3_{fluid}$ m$^{-2}_{rock}$ would only produce about 0.1 volume % or less of quartz veins, provided that all the flux was channelized into the veins. Connolly and Thompson (1989) obtained a similar result; their modeling showed that typical pervasive regional fluid fluxes are insufficient to precipitate significant amounts of quartz veins.

Our results indicating large fluid-rock ratios and q_{TI} values for vein formation are actually fully consistent with Beitter et al.'s volumetric fluid-rock ratio. To estimate the q_{TI} required to precipitate the Alpe Sponda veins, the vein fluid-rock ratio of ~1,500 m$^3_{fluid}$ m$^{-3}_{rock}$ must be multiplied by the length scale of flow (Eq. 4). Taking a representative regional length

scale of 1,000 m yields a time-integrated fluid flux of the order 10^6 m^3_{fluid} m^{-2}_{rock}, a large value

that is comparable to our estimates (Table 3; Fig. 9). Thus, we conclude that the formation of

quartz-kyanite veins on Unst and in the Alpe Sponda required large time-integrated fluid fluxes.

Downward fluid fluxes and fluid circulation in the deep crust are considered unlikely (Ague,

2003b), thus fluid fluxes responsible for vein formation on Unst would require the focusing of

upward flow of fluid from a larger source region (e.g., a thick sequence of devolatilizing

metasediments) into a relatively small volume of veined zone characterized by elevated

permeability. It is possible that the Hevda Thrust, an ancient fault system or shear zone, was

marked by high levels of permeability and acted as a structural control to focus fluids.

CONCLUSIONS

Using quantitative mass transfer relationships, we demonstrate that the

interaction of fluids and surrounding wall rocks during the metamorphism of the Saxa Vord

Pelites drove considerable mass transfer. Si, volatiles, alkalis, and alkaline earths were lost from

the selvages, whereas Ti, Y, and REEs were gained. Al was residually enriched and then

subsequently added to some of the selvages, indicating that the selvages were not the source of

Al for the vein-kyanite and that Al mass transport was a regional, not local, phenomenon. High-

P conditions (~0.8-1.1 GPa), as inferred from pseudosections, may have contributed to

increased Al concentrations in fluids through Na-Al-silicate complexing as well as enhanced

rutile solubility, facilitating the transport of Al and Ti in metamorphic fluids. Regional transport

of Na and K out of the local rock system is inferred from mass balance calculations involving

the volume of vein necessary to accommodate all the Na and K lost from the selvages during

alteration. Large fluid fluxes (~10^5-10^6 m^3_{fluid}/m^2_{rock}) and fluid-rock ratios (10^2-10^3

m^3_{fluid}/m^3_{rock}) are necessary to explain the geochemical alteration in the selvages and the

precipitation of kyanite and Fe-Ti oxides in the veins. Such significant fluid fluxes are indicative of regional fluid focusing along conduits and cracks. Transient periods of elevated permeability related to fracturing episodes along the ancient Hevda Thrust fault zone could have provided such a fracture network. Importantly, this study of the quartz-kyantie veins of Unst offers quantitative constraints on chemical alteration associated with high-P metamorphic fluid infiltration, providing evidence for open system fluid flow with regional scale mass transport of non-volatile elements, such as Al.

REFERENCES

Agapova, G. F., Modnikov, I. S., and Shmariovich, Y. M. 1989. Experimental study of the behavior of titanium in hot sulfide–carbonate solutions. *International Geology Review,* **31**, 424-430.

Ague, J. J. 1994a. Mass transfer during Barrovian metamorphism of pelites, south-central Connecticut. I: Evidence for changes in composition and volume. *American Journal of Science,* **294**, 989-1057.

Ague, J. J. 1994b. Mass transfer during Barrovian metamorphism of pelites, south-central Connecticut. II: channelized fluid flow and the growth of staurolite and kyanite. *American Journal of Science,* **294**, 1061-1134.

Ague, J. J. 1995. Deep-crustal growth of quartz, kyanite and garnet into large-aperture, fluid-filled fractures, north-eastern Connecticut, USA. *Journal of Metamorphic Geology,* **13**, 299-314.

Ague, J. J. 2003a. Fluid infiltration and transport of major, minor, and trace elements during regional metamorphism of carbonate rocks, Wepawaug Schist, Connecticut, USA. *Americal Journal of Science,* **303**, 753-816.

Ague, J. J. 2003b. Fluid Flow in the Deep Crust. In: *The Crust vol. 3., Treatise on Geochemistry* (eds Rudnick, R. L., Holland, H. D., Turekian, KK.), pp. 195-228. Elsevier, Oxford, UK.

Allaz, J., Maeder, X., Vannay, J., and Steck, A. 2005. Formation of aluminosilicate-bearing quartz veins in the Simano nappe (Central Alps): structural, thermobarometric, and oxygen isotope constraints. *Schweizerische Mineralogische und Petrographische Mitteilungen*, **85**, 191-214.

Anderson, G. M. and Burnham, C. W. 1967. Reactions of quartz and corundum with aqueous chloride and hydroxide solutions at high temperatures and pressures. American Journal of Science, **265**, 12-27.

Antignano, A., and Manning, C. E. 2008. Rutile solubility in H_2O, H_2O–SiO_2, and H_2O–$NaAlSi_3O_8$ fluids at 0.7–2.0 GPa and 700–1000 °C: Implications for mobility of nominally insoluble elements. *Chemical Geology,* **255**, 283-293.

Audétat, A., and Keppler, H. 2005. Solubility of rutile in subduction zone fluids, as determined by experiments in the hydrothermal diamond anvil cell. *Earth and Planetary Science Letters,* **232**, 393-402.

Ayers, J. C., and Watson, E. B. 1991. Solubility of apatite, monazite, zircon, and rutile in supercritical aqueous fluids with implications for subduction zone geochemistry: *Philosophical Transactions of the Royal Society of London Series A*, **335**, 365–375.

Ayers, J. C., and Watson, E. B. 1993. Rutile solubility and mobility in supercritical aqueous fluids. *Contributions to Mineralogy and Petrology,* **114**, 321-330.

Barton, C. A., Zoback, M. D., and Moos, D. 1995. Fluid flow along potentially active faults in crystalline rock. *Geology*, **23**, 683-686.

Bau, M. 1991. Rare-earth element mobility during hydrothermal and metamorphic fluid-rock interaction and the significance of the oxidation state of europium. *Chemical Geology*, **93**, 219-230.

Bau, M. and Dulski, P. 1995. Comparative study of yttrium and rare-earth element behaviors in fluorine-rich hydrothermal fluids. *Contributions to Mineralogy and Petrology*, **119**, 213-223.

Bebout, G. E. and Barton, M. D. 1993. Metasomatism during subduction: products and possible paths in the Catalina Schist, California. *Chemical Geology*, **108**, 61-92.

Becker, H., Jochum, K. P., and Carlson, R. W. 1999. Constraints from high-pressure veins in eclogites on the composition of hydrous fluids in subduction zones. *Chemical Geology*, **160**, 291-308.

Beitter, T., Wagner, T., and Markl, G. 2008. Formation of kyanite-quartz veins of the Alpe Sponda, Central Alps Switzerland: implications for Al transport during regional metamorphism. *Contributions to Mineralogy and Petrology*, **156**, 689-707.

Bickle, M. J. 1992. Transport Mechanisms by Fluid-Flow in Metamorphic Rocks: Oxygen and Strontium Decoupling in the Troi Seigneurs Massif-A Consequence of Kinetic Dispersion? *American Journal of Science*, **292**, 289-316.

Boulvais, P., Fourcade, S., Moine, B., Gruau, G., and Cuney, M. 2000. Rare-earth elements distribution in granulites-facies marbles: a witness of fluid-rock interaction. *LIthos*, **53**, 117-126.

Breeding, C. M. and Ague, J. J. 2002. Slab-derived fluids and quartz-vein formation in an accretionary prism, Otago Schist, New Zealand. *Geology*, **30**, 499-502.

Breeding, C. M., Ague, J. J., Grove, M., and Rupke, A. L. 2004. Isotopic and chemical alteration of zircon by metamorphic fluids: U-Pb age depth-profiling of zircon crystals from Barrow's garnet zone, northeast Scotland. *American Mineralogist*, **89**, 1067-1077.

Bröcker M. and Enders M. 2001. Unusual bulk-rock compositions in eclogite-facies rocks from Syros and Tinos (Cyclades, Greece): implications for U–Pb zircon geochronology. *Chemical Geology*, **175**, 581-603.

Burnham, C. W., Ryzhenko, B. N., and Schitel, D. 1973. Water solubility of corundum at 500-800 ºC and 6 kbar. *Geochemistry International*, **10**, 1374.

Carmichael, D. M. 1969. On the mechanism of prograde metamorphic reactions in quartz-bearing pelitic rocks. *Contributions to Mineralogy and Petrology*, **146**, 275-285.

Carlson, W. D. 2002. Scales of disequilibrium and rates of equilibration during metamorphism: *American Mineralogist*, **87**, 185–204.

Connolly, J. A. D. and Thompson, A. B. 1989. Fluid and enthalpy production during regional metamorphism. *Contributions to Mineralogy and Petrology*, **102**, 347-366.

Diakonov, I., Pokrovski, G., Schott, J., Castet, S., and Gout, R. 1996. An experimental and computational study of sodium-aluminum complexing in crustal fluids. *Geochimica et Cosmochimica Acta*, **60**, 197-211.

Dipple, G. M., and Ferry, J. M. 1992. Metasomatism and fluid flow in ductile fault zones. *Contributions to Mineralogy and Petrology*, **112**, 149-164.

Dunning, G. R. and Pedersen, R. B. 1988. U/Pb ages of ophiolites and arc-related plutons of the Norwegian Caledonides: implications for the development of Iapetus. *Contributions to Mineralogy and Petrology*, **98**, 13-23.

Etheridge, M. A., Wall, V. J., and Vernon, R. H. 1983. The role of the fluid phase during regional metamorphism and deformation. *Journal of Metamorphic Geology*, **1**, 205-226.

Ferry, J. M. 1994. Overview of the Petrologic Record of Fluid Flow During Regional Metamorphism in Northern New England. *American Journal of Science*, **294**, 905-988.

Ferry J. M. 1988. Contrasting mechanisms of fluid flow through adjacent stratigraphic units during regional metamorphism, south-central Maine, USA. *Contributions to Mineralogy and Petrology*, **98**, 1–12.

Flinn, D., Key, R. M., and Khoo, T. T. 1996. The chloritoid schists of Shetland and their thermal metamorphism. *Scottish Journal of Geology*, **32**, 67-82.

Flinn, D. and. Oglethorpe, R. J. D. 2005. A history of the Shetland Ophiolite Complex. *Scottish Journal of Geology*, **41**, 141-148.

Flinn, D. 2007. The Dalradian rocks of Shetland and their implications for the plate tectonics of the northern Iapetus. *Scottish Journal of Geology*, **43**, 125-142.

Franz L., Romer R.L., Klemd R., Schmid R., Oberhänsli R., Wagner T., and Schuwen, D. 2001. Eclogite–facies quartz veins within metabasites of the Dabie Shan (eastern China): pressure–temperature–time–deformation path, composition of the fluid phase and fluid flow during exhumation of high-pressure rocks. *Contribution to Mineralogy Petrology,* **141**, 322–346

Gao, J. and Klemd, R. 2001. Primary fluids entrapped at blueschist to eclogite transition: evidence from the Tianshan meta-subduction complex in northwestern China. *Contribution to Mineralogy Petrology,* **142**, 1-14.

Gao, J., John, T., Klemd, R., and Xiong, X. 2007. Mobilization of Ti–Nb–Ta during subduction: evidence from rutile-bearing dehydration segregations and veins hosted in eclogite, Tianshan, NWChina. *Geochimica et Cosmochimica Acta*, **71**, 4974-4996.

Garson, M. S., and Plant, J. A. 1973. Alpine type ultramafic rocks and episodic mountain building in the Scottish Highlands. *Nature,* **242**, 34-38.

Gieré, R. and Williams, C. T. 1992. REE-bearing minerals in a Ti-rich vein from the Adamello contact aureole (Italy). *Contributions to Mineralogy and Petrology*, **112**, 83-100.

Grant J. A. 1986 The isocon diagram—a simple solution to Gresens'equation for metasomatic alteration. *Economic Geology*, **81**, 1976–1982.

Heinrich, C. A. 1986. Eclogite Fades Regional Metamorphism of Hydrous Mafic Rocks in the Central Alpine Adula Nappe. *Journal of Petrology*, **27**, 123-154.

Holland, T. J., and Powell, R. 1998. An internally consistent thermodynamic data set for phases of petrological interest. *Journal of Metamorphic Geology*, **16**, 309-343.

Jiang, S., Wang, R., Xu, X., and Zhao, K. 2005. Mobility of high field strength elements HFSE in magmatic-, metamorphic-, and submarine-hydrothermal systems. *Physics and Chemistry of the Earth*, **30**, 1020-1029.

Kerrick, D. M. 1990. *The Al2SiO5 Polymorphs: Reviews in Mineralogy, Volume 22.* Washington, D.C.: Mineralogical Society of America.

Kerrick, D. M., and Jacobs, G. K. 1981. A modified Redlich-Kwong equation for H2O, CO2, and H2O-CO2 mixtures at elevated pressures and temperatures. *American Journal of Science*, **281**, 736-767.

Manning, C. E. 1994. The solubility of quartz in H2O in the lower crust and upper mantle. *Geochimica et Cosmochimica Acta*, **58**, 4831-4839.

Manning, C. E. 2006. Mobilizing aluminum in crustal and mantle fluid. *Journal of Geochemical Exploration*, **89**, 251-253.

Manning, C. E. 2007. Solubility of corundum + kyanite in H2O at 700ºC and 10 kbar: evidence for Al-Si complexing at high pressure and temperature. *Geofluids*, **7**, 258-269.

Masters, R. L., and Ague, J. J. 2005. Regional-scale fluid flow and element mobility in Barrow's metamorphic zones, Stonehaven, Scotland. *Contributions to Mineralogy and Petrology*, **150**, 1-18.

McLelland, J., Morrison, J., Selleck, B., Cunningham, B., Olson, C., and Schmidt, K. 2002. Hydrothermal alteration of late- to post- tectonic Lyon Mountain granitic gneiss, Adirondack Mountains, New York: origin of quartz-sillimanite segregations, quartz-albite lithologies, and associated Kiruna-type low-Ti-Fe-oxide deposits. *Journal of Metamorphic Geology*, **20**, 175-190.

McLelland, J., Morrison, J., Selleck, B., Cunningham, B., Olson, C., and Schmidt, K. 2002. Hydrothermal alteration of late- to post-tectonic Lyon Mountain Granitic Gneiss, Adirondack Mountains, New York: Origin of quartz–sillimanite segregations, quartz–albite lithologies, and associated Kiruna-type low-Ti Fe-oxide deposits. *Journal of Metamorphic Geology*, **20**, 175-190.

Molina, J. F., Poli, S., Austrheim, H., Glodny, J., and Rusin, A. 2004. Eclogite-facies vein systems in the Marun-Keu complex (Polar Urals, Russia): textural, chemical and thermal constraints for patterns of fluid flow in the lower crust. *Contributions to Mineralogy and Petrology*, **147**, 484-504.

Mykura, W. 1976. *British Regional Geology: Orkney and Shetland.* Edinburgh: Natural Environment Research Council, Institute of Geological Science.

Nabelek, P. 1997. Quartz-sillimanite leucosomes in high-grade schists, Black Hills, South Dakota: a perspective on the mobility of Al in high-grade metamorphic rocks. *Geology*, **25**, 995-998.

Nelson, B. K. 1995. Fluid flow in subduction zones: evidence from Nd- and Sr-isotope variations in metabasalts of the Franciscan complex, California. *Contributions to Mineralogy and Petrology*, **119**, 247-262.

Newton, R., and Manning, C. 2006. Activity coefficient and polymerization of silica at 800 °C, 12 kbar, from solubility measurements on SiO_2-buffering mineral assemblages. *Contributions to Mineralogy and Petrology*, **146**, 135-143.

Oliver, N. H., Dipple, G. M., Cartwright, I., and Schiller, J. 1998. Fluid flow and metasomatism in the genesis of the amphibolite-facies, pelite-hosted Kanmantoo copper deposit, South Australia. *American Journal of Science*, **298**, 181-218.

Pan, Y. and Fleet, M. E. 1996. Rare earth element mobility during prograde granulite facies metamorphism: significance of fluorine. *Contributions to Mineralogy and Petrology*, **123**, 251-262.

Penniston-Dorland, S. C., and Ferry, J. M. 2008. Element mobility and scale of mass transport in the formation of quartz veins during regional metamorphism of the Waits River Formation, east-central Vermont. *American Mineralogist*, **93**, 7-21.

Philippot, P., and Selverstone, J. 1991. Trace-element-rich brines in eclogitic veins — implications for fluid composition and transport during subduction. *Contributions to Mineralogy and Petrology*, **106**, 417-430.

Philpotts, A. and Ague, J. J. 2009. *Principles of Igneous and Metamorphic Petrology, 2nd Edition*. Cambridge University Press, Cambridge, UK.

Powell, R., Holland, T. J., and Worley, B. 1998. Calculating phase diagrams involving solid solutions via non-linear equtions, with examples using THERMOCALC. *Journal of Metamorphic Geology*, **16**, 577-588.

Putlitz, B., Valley, J. W., Matthews, A., Katzir, Y. 2002. Oxygen isotope thermometry of quartz–Al2SiO5 veins in high-grade metamorphic rocks on Naxos Island (Greece). *Contributions to Mineralogy and Petrology*, **143,** 350-359.

Ragnarsdottir, K. V., and Walther, J. V. 1985. Experimental determination of corundum solubilities in pure water between 400-700ºC and 1-3 kbars. *Geochimica et Cosmochimica Acta*, **48**, 159-176.

Read, H. H. 1932. On quartz-kyanite-rocks in Unst, Shetland Islands, and their bearing of metamorphic differentiation. *Mineralogical Magazine*, **23**, 317-328.

Read, H. H. 1934. On zoned associations of antigorite, talc, actinolite, chlorite, and biotite in Unst, Shetland Islands. *Journal of the Mineralogical Society*, **145**, 519-540.

Rubatto, D. and Herman, J. 2003. Zircon formation during fluid circulation in eclogites (Monviso, Western Alps): Implications for Zr and Hf budget in subduction zones. *Geochimica et Cosmochimica Acta*, **67**, 2173-2187.

Salvi, S., Pokrovski, G. S., and Schott, J. 1998. Experimental investigation of aluminum-silica aqueous complexing at 300ºC. *Chemical Geology*, **151**, 51-67.

Schuiling, R. D. and Vink, B. W. 1967. Stability relations of some titanium-minerals (sphene, perovskite, rutile, anatase). *Geochimica et Cosmochimica Acta*, **31**, 2399-2411.

Selverstone, J., Morteani, G., and Staude, J.-M. 1991. Fluid channeling during ductile shearing: transformation of granodiorite into aluminous schist in the Tauern Window, Eastern Alps. *Journal of Metamorphic Geology*, B, 419-432.

Selverstone, J., Franz, G., Thomas, S., and Getty, S. 1992. Fluid variability in 2 GPa eclogites as an indicator of fluid behavior during subduction. *Contributions to Mineralogy and Petrology*, **112**, 341-357.

Sepahi, A. A., Whitney, D. L., and Baharifar, A. A. 2004. Petrogenesis of andalusite-kyanite-sillimanite veins and host rocks, Sanandaj-Sirjan metamorphic belt, Hamadan, Iran. *Journal of Metamorphic Geology*, **22**, 119-134.

Skelton, A. D. L., Valley, J. W., Graham, C. M., Bickle, M. J., and Fallick, A. E. 2000. The correlation of reaction and isotope fronts and the mechanism of metamorphic fluid flow. *Contributions to Mineralogy and Petrology*, **138**, 364-375.

Snelling, N. J. 1957. A contribution to the mineralogy of chloritoid. *Mineralogical Magazine*, **31**, 469-75.

Snelling, N. J. 1958. Further data on the petrology of the Saxa Vord schists on Unst, Shetland Isles. *Geological Magazine*, **95**, 50-56.

Sorensen, S. S., and Grossman, J. N. 1989. Enrichment of trace-elements in garnet amphibolites from a paleo-subduction zone — Catalina Schist, Southern-California. *Geochimica et Cosmochimica Acta*, **53**, 3155-3177.

Tagirov, B., and Schott, J. 2001. Aluminum speciation in crustal fluids revisited. *Geochimica et Cosmochimica Acta*, **65**, 3965-3992.

Thompson, A. B. 1975. Calc–silicate diffusion zones between marble and pelitic schist. *Journal of Petrology*, **16**, 314–346

Tropper, P., and Manning, C. 2007. The solubility of corundum in H2O at high pressure and temperature and its implications for Al mobility in the deep crust and upper mantle. *Chemical Geology*, **240**, 54-60.

van Baalen, M. R. 1993. Titanium mobility in metamorphic systems: a review. *Chemical Geology*, **110**, 233-249.

Verlaguet, A., Brunet, F., Goffé, B., and Murphy, W. M. 2006. Experimental study and modeling of fluid reaction paths in the quartz–kyanite ± muscovite–water system at 0.7 GPa in the 350–550 °C range: Implications for Al selective transfer during metamorphism. *Geochimica et Cosmochimica Acta*, **70**, 1772-1788.

Walther, J. V. 1997. Experimental determination and interpretation of the solubility of corundum in H2O between 350 and 600ºC from 0.5 to 2.2 kbar. *Geochimica et Cosmochimica Acta*, **61**, 4955-4964.

Walther, J. V. 2001. Experimental determination and analysis of the solubility of corundum in 0.1 and 0.5 m NaCl solutions between 400 and 600°C from 0.5 to 2.0 kbar. *Geochimica et Cosmochimica Acta*, **65**, 2843-2851.

Whitney, D. L and Olmsted, J. F. 1998. Rare earth element metasomatism in hydrothermal systems: The Willsboro-Lewis wollastonite ores, New York, USA. *Geochimica et Cosmochimica Acta*, **62**, 2965-2977.

Whitney, D. L., and Dilek, Y. 2000. Andalusite-sillimanite-quartz veins as indicators of low-pressure-high-temperature deformation during late-stage unroofing of a metamorphic core complex, Turkey. *Journal of Metamorphic Geology*, **18**, 59-66.

Widmer, T. and Thompson, A. B. 2001. Local origin of high-pressure vein material in eclogite facies rocks of the Zermatt-Saas zone, Switzerland. *American Journal of Science*, **301**, 627-656.

Wood, B. J. and Walther, J. V. 1986. Fluid Flow during Metamorphism and its Implications for Fluid-Rock Ratios. In: *Fluid-rock Interactions during Metamorphism* (eds Walther, J. V. and Wood, B. J.), pp. 89-108. Springer, New York.
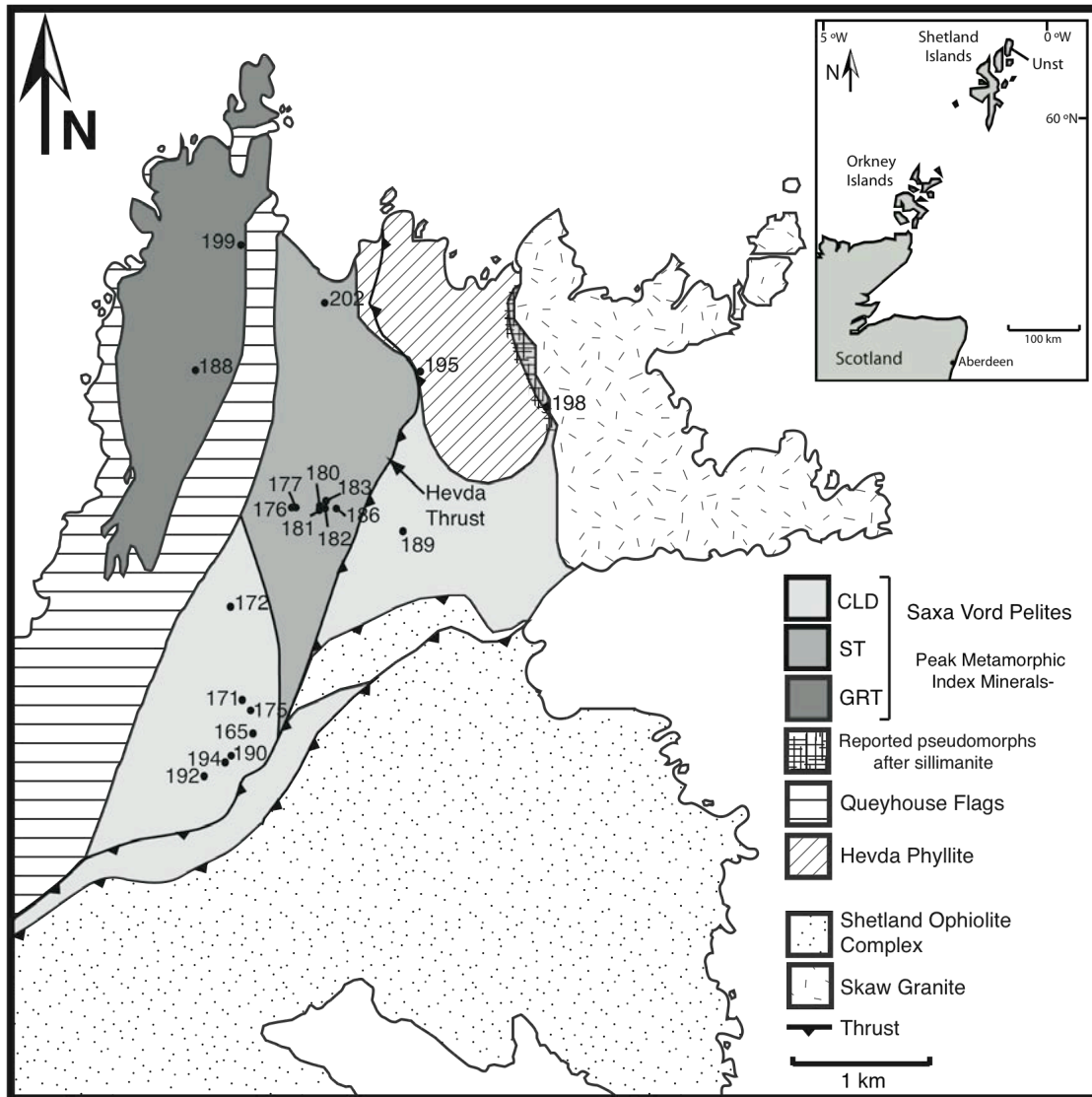
Fig. 1 Simplified geological map of the NE corner of Unst showing the major lithological units and structural features. The inset shows the regional context of the Shetland Islands. Mineral abbreviations in all figures after Kretz (1983). Sample numbers begin with prefix JAB. Index mineral zones for the Saxa Vord Pelites based on sampling. See text for description of the lithological units.
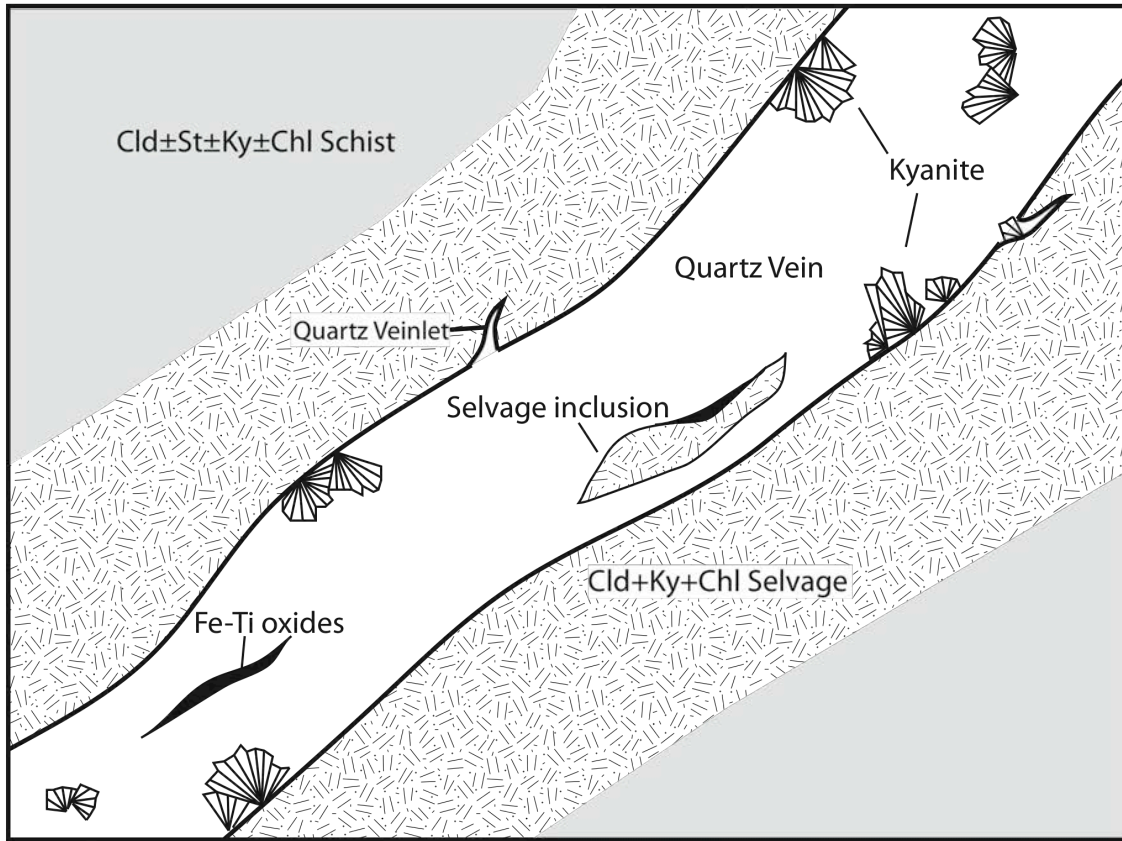
Fig. 2 Schematic sketch (not to scale) of the lithologies around the quartz-kyanite veins of the Saxa Vord Pelite, including precursor schists and altered selvages. Note inclusions of selvages, large Fe-Ti oxides, and abundant splays of kyanite in veins. Also, small quartz veinlets branching off from large quartz veins may infiltrate the surrounding selvages.
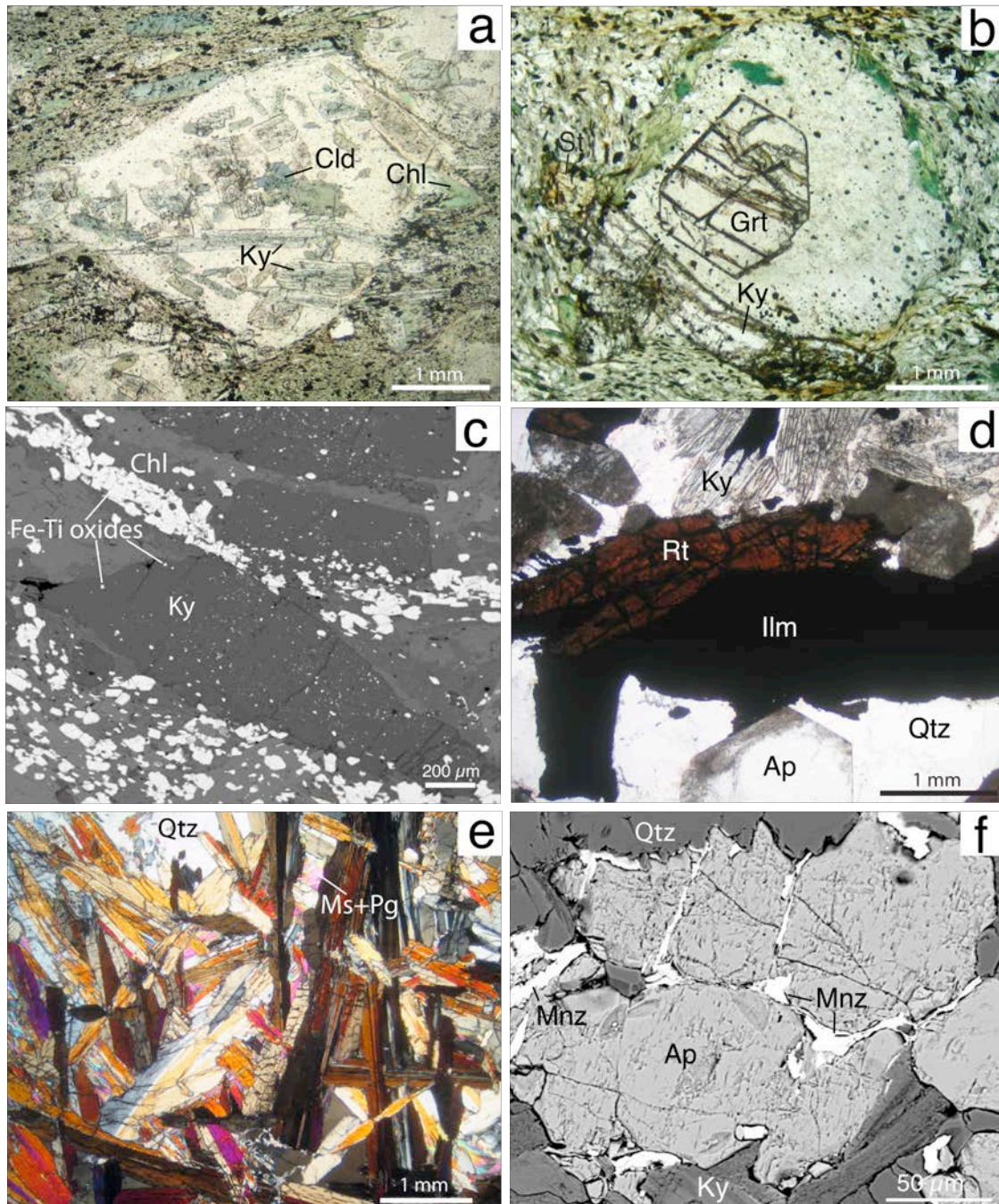
Fig. 3 Representative photomicrographs of typical assemblages found in the field. a) Pseudomorph replaced by Cld+Ky+Chl in selvage sample JAB181E (plane polarized light). Note high percentage of Fe-Ti oxides in surrounding matrix. b) Ovoid pseudomorph replaced by white mica and large Grt porphyroblast from sample JAB188A (plane polarized light). Note the bent Ky crystal and St in surrounding matrix. c) Back-scatter electron image of selvage sample JAB181A. Note large Ky crystals with inclusions of Fe-Ti oxides and surrounding bands of Chl and Fe-Ti oxides. d) Quartz vein with Rt rimmed by Ilm as well as large Ap and Ky crystals from sample JAB176A2 (plane polarized light). e) Splays of Ky from vein sample JAB181A. Note retrograde growth of Ms+Pg around Ky crystals (cross-polarized light). f) Back-scatter electron image of fractured Ap crystal with Mnz overgrowths in Qtz-Ky vein from sample JAB181A.
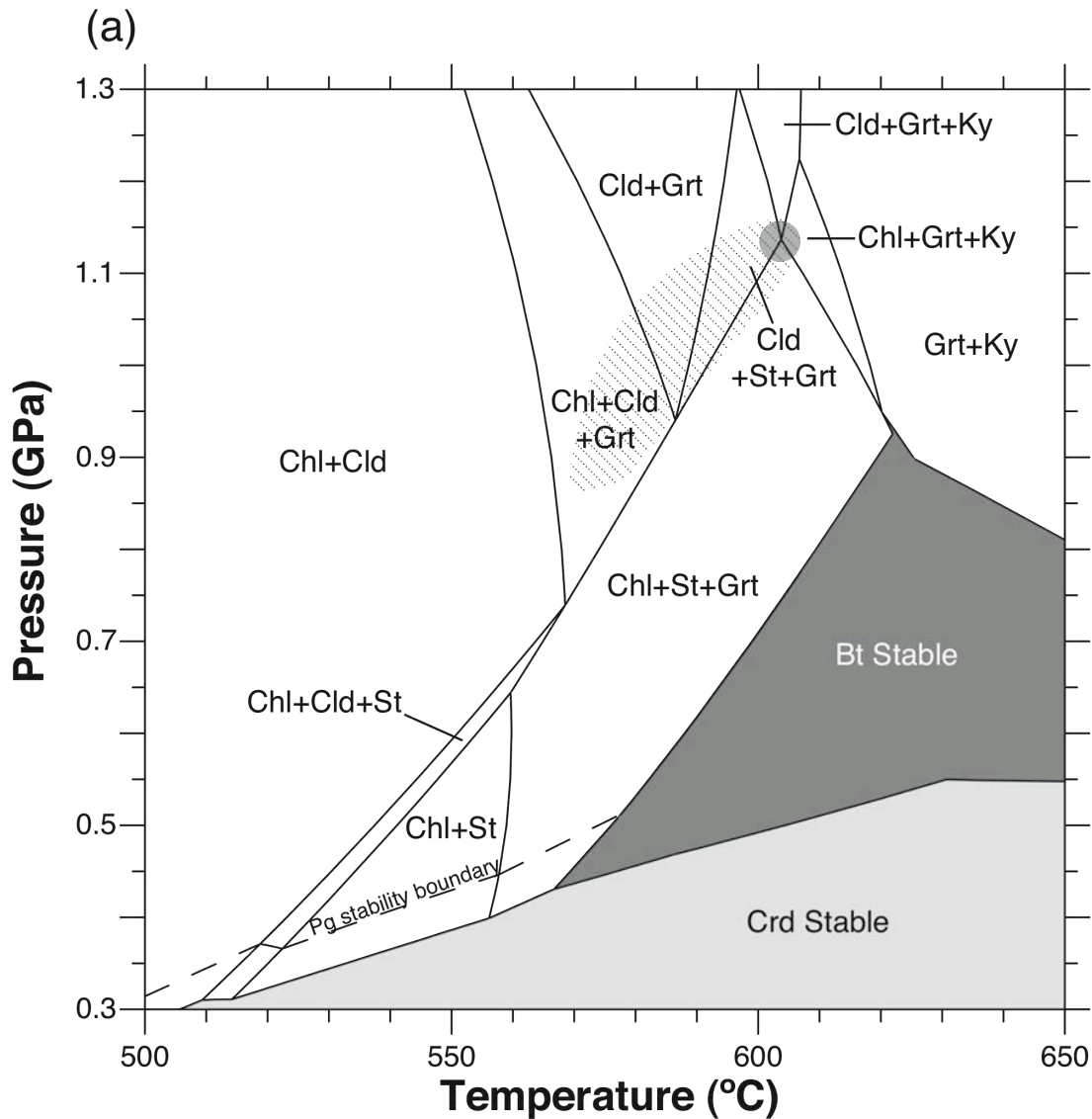
Fig. 4 NKFMASH *P-T* pseudosection for representative precursor composition of sample JAB165A2. All equilibrium assemblages also have the unlabeled phases of Ms, Pg, Qtz, and H_2O, except for those below the Pg stability field, which do not have Pg. Simplified Bt, Crd, & And stability fields are shown for reference. The gray circle indicates the *P-T* invariant point where Chl+Cld+St+Grt+Ky coexist. (a) *P-T* pseudosection calculated assuming that all Fe from XRF analyses was in the Fe^{2+} state. (b) *P-T* pseudosection calculated assuming that 75 mole % Fe from the XRF analyses was in the Fe^{2+} state and the remainder was in the Fe^{3+} state. The *P-T* metamorphic field gradient is shown as a stippled area.

(b)
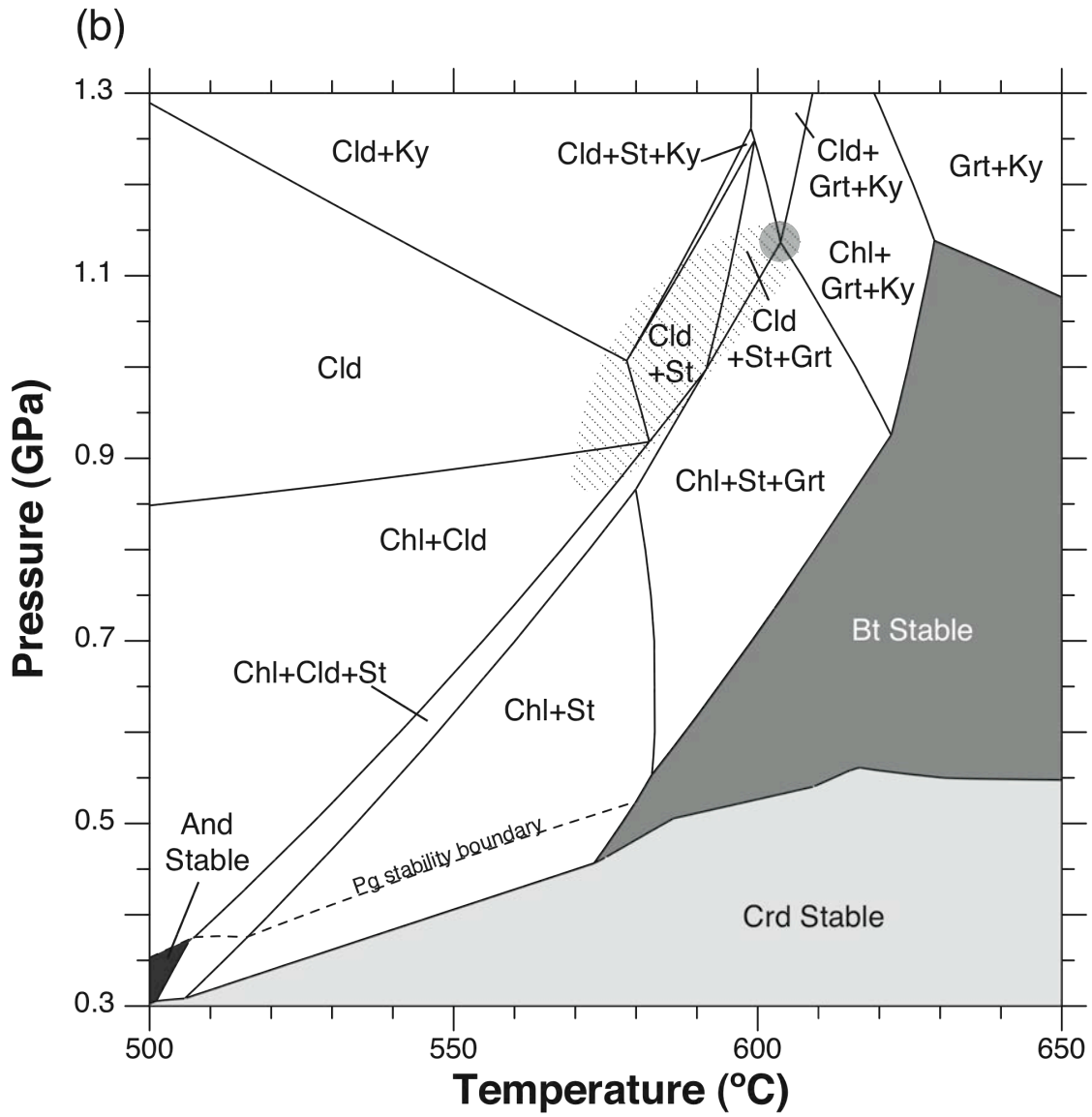
Fig. 4 (continued)
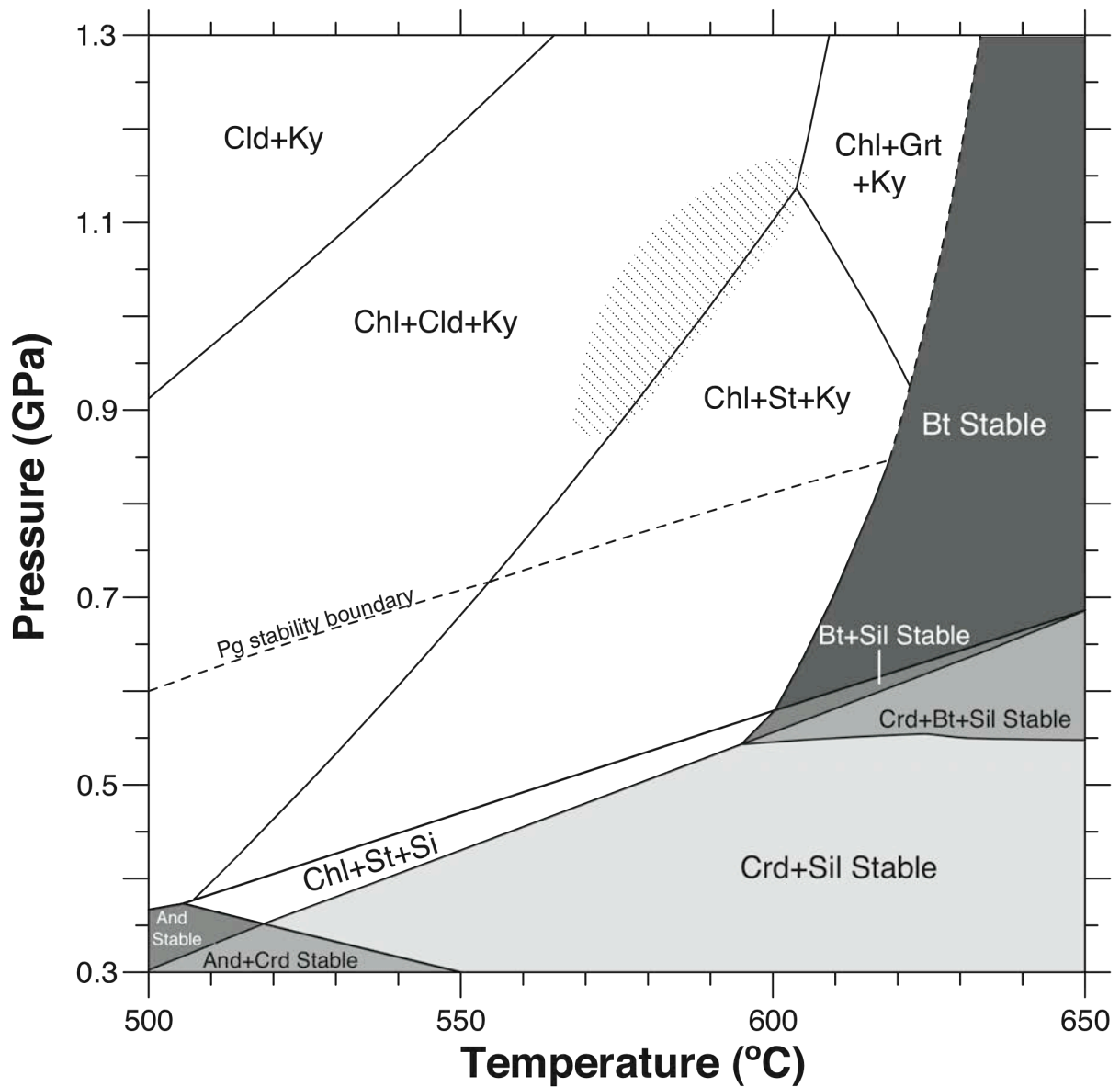
Fig. 5 NKFMASH *P-T* pseudosection for representative selvage composition of sample JAB181Aiii. All equilibrium assemblages also have the unlabeled phases of Ms, Pg, Qtz, and H_2O, except for those below the Pg stability field, which do not have Pg. Simplified Bt, Crd, Sil, & And stability fields are shown for reference. The *P-T* metamorphic field gradient from is shown as a stippled area.
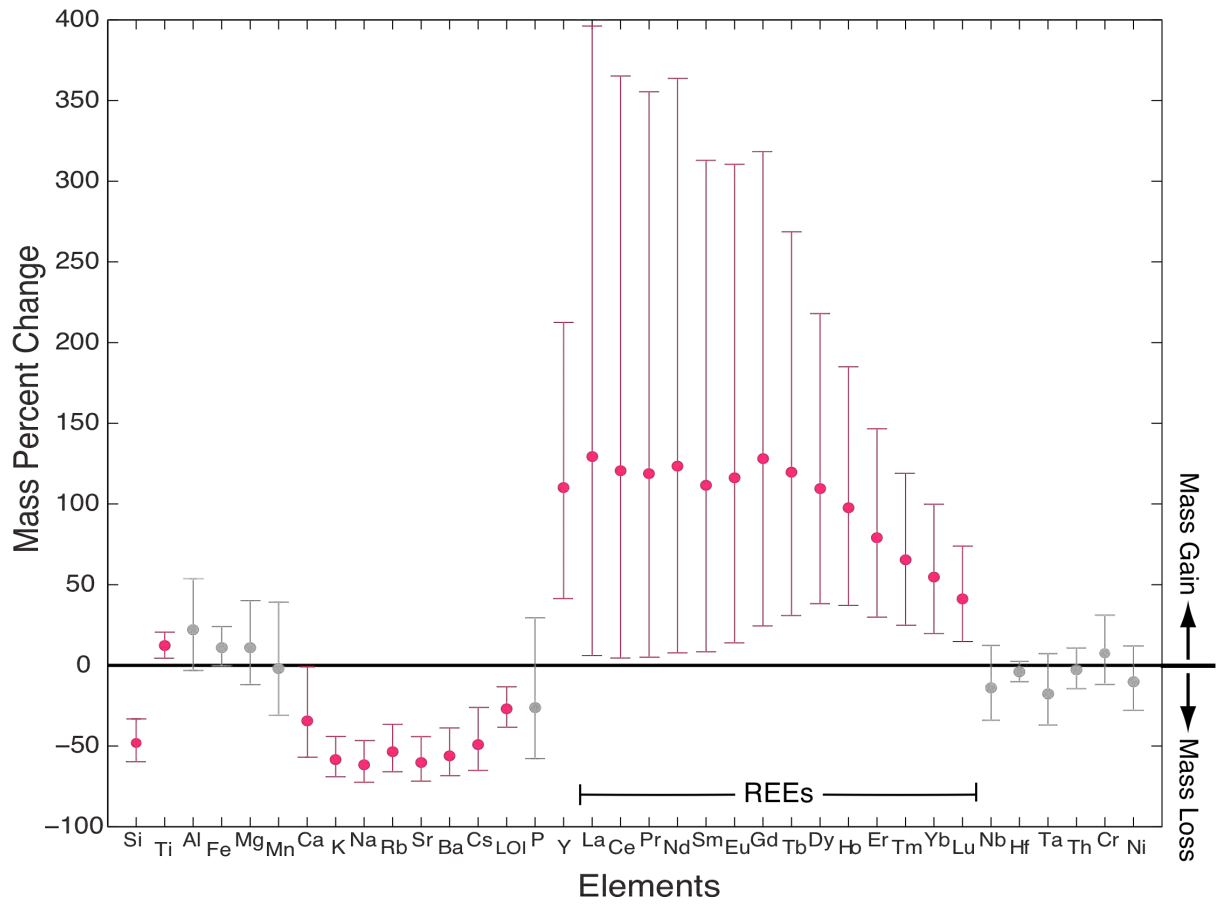
Fig. 6 Mass percent change diagram for altered selvages relative to precursors using Zr as a reference element. Calculations are described in the text. Statistically significant mass changes are shown in red and non-statistically significant mass change in grey.
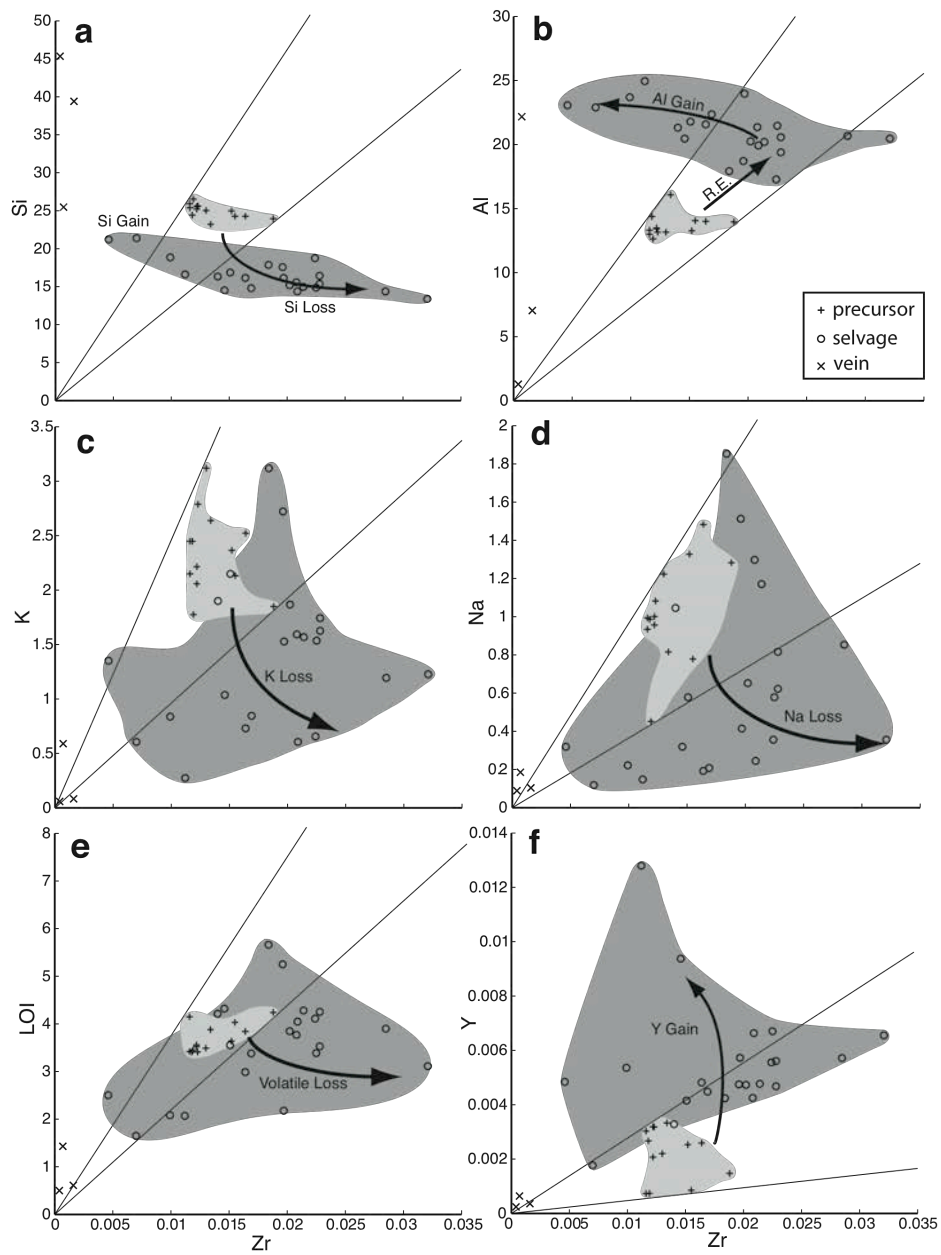
Fig. 7 Wedge diagrams for Si, Al, Na, K, volatiles (LOI), and Y. Plus symbols denote precursor samples, circles denote selvage samples, and crosses are veins samples. The light grey and dark grey areas highlight the clouds of precursor and selvage data points, respectively. Arrows indicates mass loss, addition, or residual enrichment (R.E.) trends.
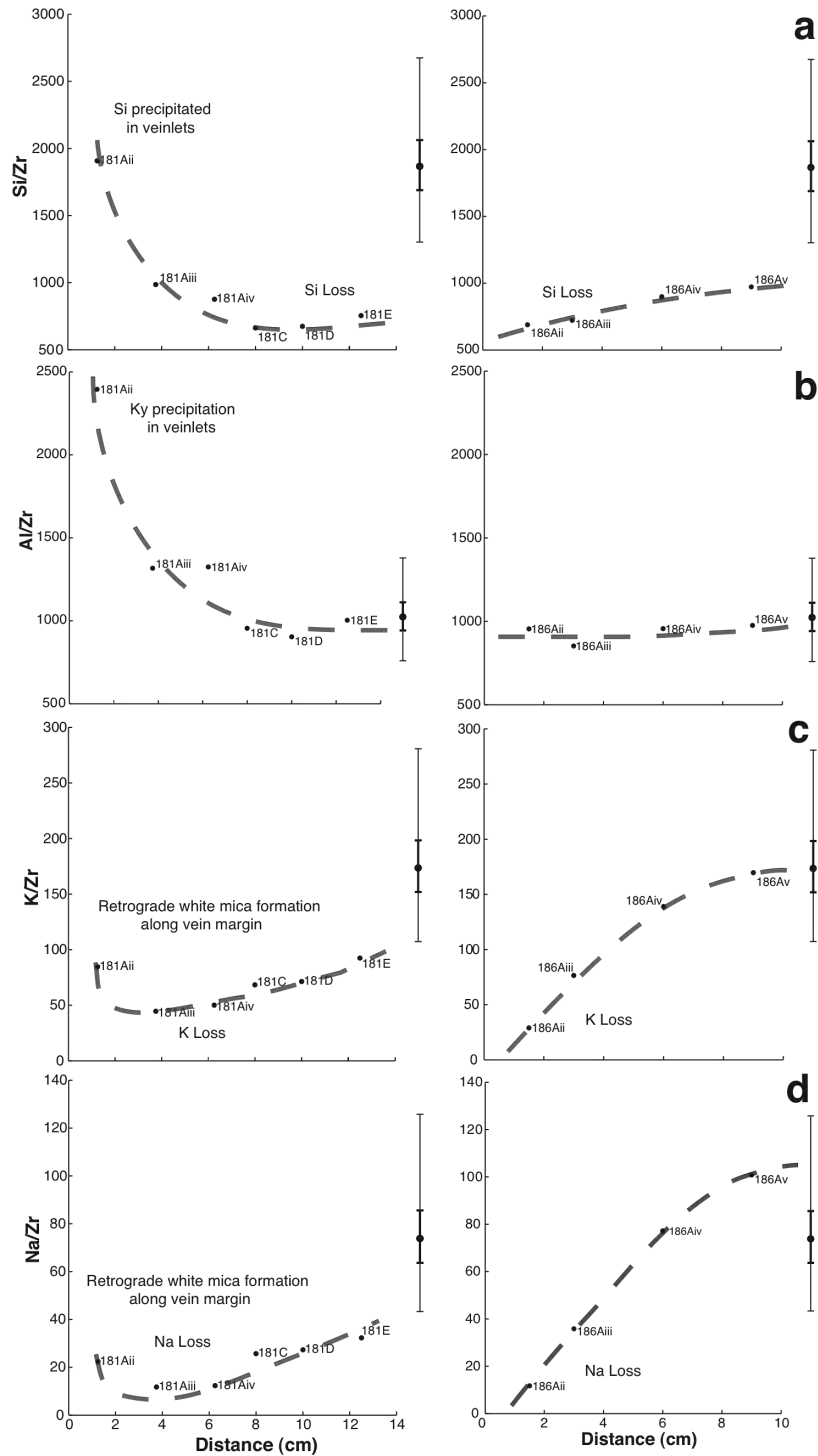
Fig. 8 Geochemical traverses for sample sites 181 and 186. Contact with vein at 0 cm. The geometric mean of precursor samples is indicated with a dot to the right side of the traverses. Standard deviations of the mean and standard deviation of the population are indicated by thick and thin bracketed error bars, respectively. (a) Si/Zr, (b) Al/Zr, (c) K/Zr, (d) Na/Zr, (e) Rb/Zr, (f) Ba/Zr, (g) Sr/Y, and (h) La/Zr shown (continued on next page). ICP-MS values used for Y.

e

Rb/Zr

Retrograde white mica formation along vein margin

181Aii

181Aiii

181Aiv

181C

181D

181E

Rb loss

Rb loss

186Aii

186Aiii

186Aiv

186Av

f

Ba/Zr

Retrograde white mica formation along vein margin

181Aii

181Aiii

181Aiv

181C

181D

181E

Ba loss

186Aii

186Aiii

186Aiv

186Av

Ba loss

g

Sr/Y

Sr loss and Y gain

181Aii

181Aiii

181Aiv

181C

181D

181E

Sr loss and Y gain

186Aii

186Aiii

186Aiv

186Av

h

La/Zr

181Aii

La Gain

181Aiii

181Aiv

181C

181D

181E

186Aii

186Aiii

186Aiv

186Av

Distance (cm)

Distance (cm)

Fig. 8 (continued)

48

Fig. 9 Graph of calculated time-integrated fluid fluxes versus distance of front propagation (see Table 3). Gray region indicates time-integrated fluid fluxes for regional fluid transport (L=1000 m).

Table 1: Major oxides, minor oxides, LOI, Rb, Sr, Ba, Zr, Nb, and Y[a]

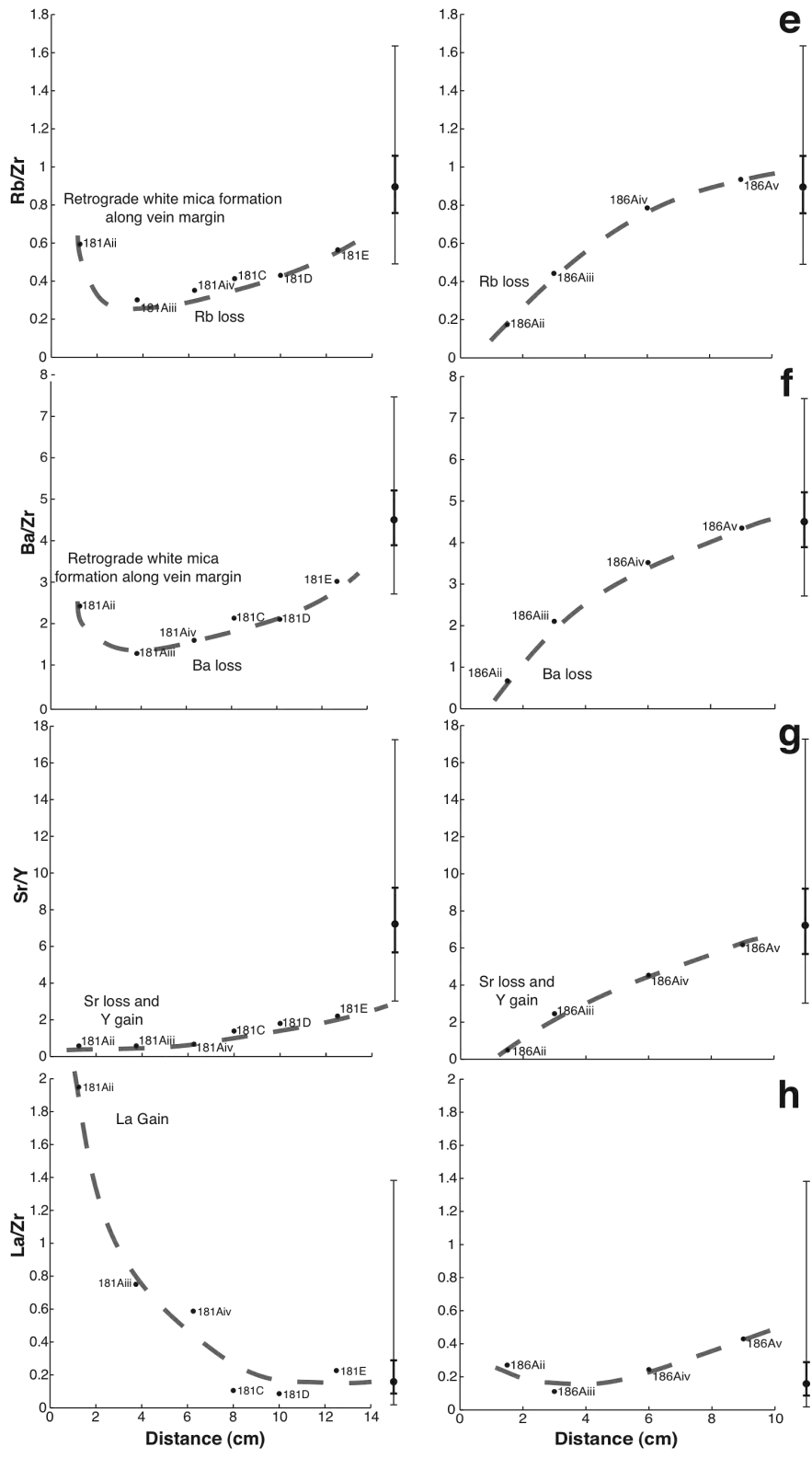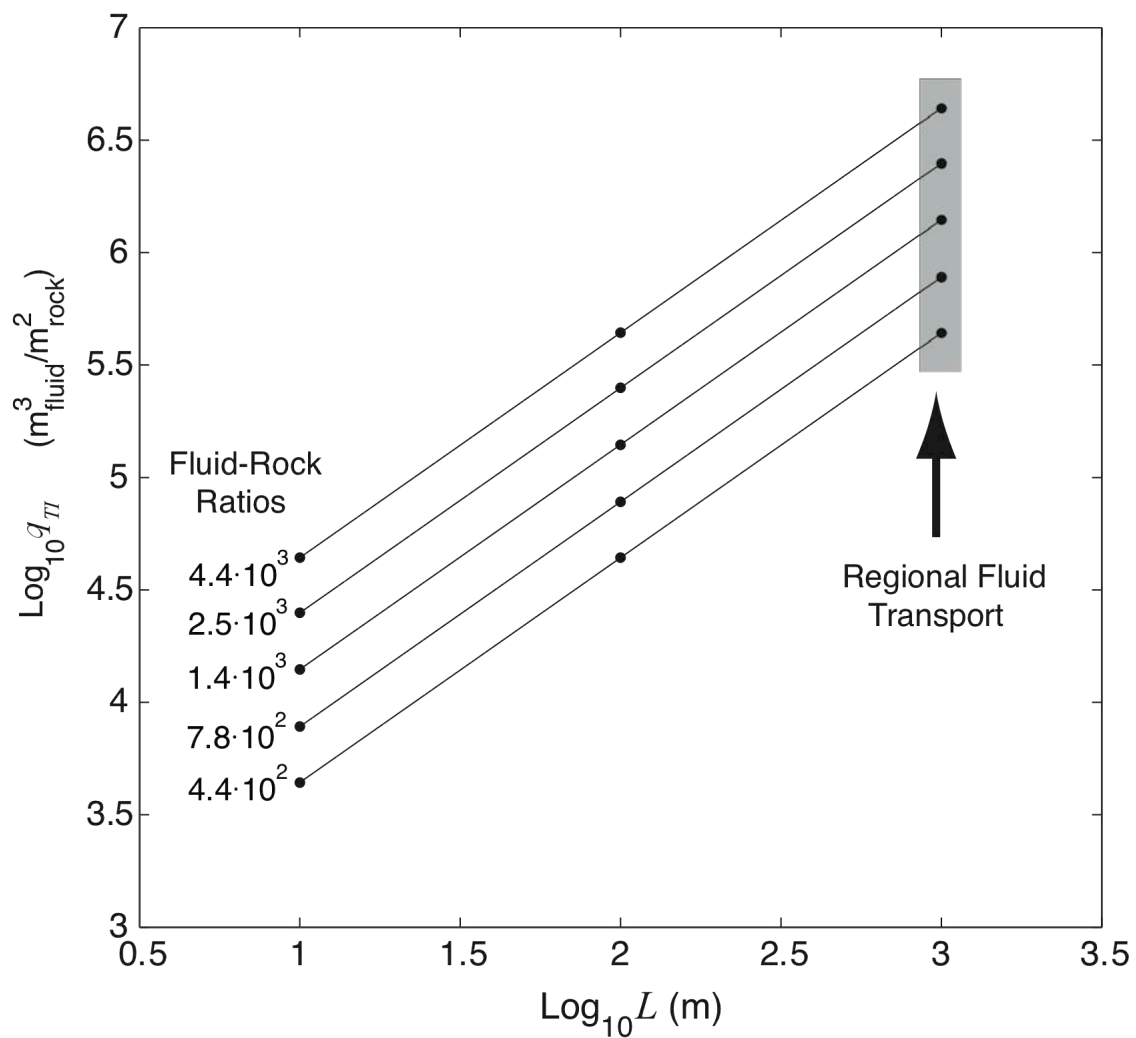| Sample #	R.C.[b]	X[c]	SiO_2	TiO_2	Al_2O_3	Fe_2O_3	MgO	MnO	CaO	K_2O	Na_2O	P_2O_5	LOI	Total[d]	Rb	Sr	Ba	Zr	Nb	Y
165A2	0	-	52.0	0.98	26.6	9.63	1.98	0.11	0.46	2.57	1.05	0.09	4.03	99.6	100	107	520	155	15	8
165A3	0	-	56.8	0.89	23.9	10.1	1.48	0.24	0.41	2.14	0.61	0.08	3.45	100.1	86	62	590	119	16	6
171A	0	-	54.0	0.92	25.4	9.43	1.51	0.19	0.55	2.67	1.35	0.16	3.52	99.7	122	142	560	122	16	28
172A	0	-	54.4	0.91	24.6	8.90	1.97	0.14	0.51	2.95	1.34	0.08	4.15	100.0	127	132	660	116	15	7
175Ai	2	-	97.0	0.02	2.44	0.28	0.05	b.d.	0.06	0.07	0.12	b.d.	0.50	100.5	3	4	b.d.	4	b.d.	b.d.
175Aiii	1	-	35.0	1.13	40.3	11.8	2.38	0.34	0.53	2.29	1.41	0.20	4.21	99.6	109	123	470	140	21	30
176A1	1	-	31.1	1.17	38.7	14.0	4.83	0.23	1.86	1.25	0.43	1.31	4.32	99.2	64	59	410	146	12	80
176A2i	1	-	45.4	0.48	43.6	4.15	1.17	0.04	0.44	1.63	0.43	0.29	2.50	100.2	83	49	420	46	10	40
177A	1	-	30.8	2.16	39.1	19.2	1.82	0.52	0.62	1.44	1.15	0.04	3.90	100.8	68	136	350	285	83	47
180B	1	-	28.7	2.48	38.7	22.9	2.00	0.59	0.15	1.48	0.48	0.03	3.11	100.6	74	44	330	321	16	59
181Ai	2	-	84.3	0.10	13.3	0.99	0.06	0.03	0.05	0.1	0.14	0.03	0.61	99.8	5	9	-20	16	2	3
181Aii	1	1.25	40.4	0.90	44.8	8.30	1.51	0.13	0.38	1.01	0.30	0.28	2.08	100.2	51	31	240	99	12	45
181Aiii	1	3.75	34.6	1.56	40.8	15.0	3.00	0.27	0.26	0.88	0.26	0.20	2.99	99.8	45	28	210	164	19	39
181Aiv	1	6.25	31.7	1.49	42.3	15.9	3.20	0.42	0.26	1.02	0.28	0.15	3.38	100.1	51	30	270	169	20	39
181C	1	8	31.9	1.81	40.6	15.9	2.92	0.15	0.48	1.85	0.78	0.11	3.39	100.0	86	93	480	225	17	57
181D	1	10	32.9	1.96	38.9	16.4	2.61	0.14	0.46	1.96	0.84	0.10	3.53	99.8	89	101	480	228	18	47
181E	1	12.5	32.6	1.69	38.3	16.1	3.58	0.16	0.47	2.25	0.88	0.16	3.85	100.2	107	104	610	202	14	41
182A	1	-	34.6	1.85	45.3	13.6	1.29	0.04	0.07	1.84	0.56	0.02	2.18	101.4	98	61	380	197	14	49
183A	1	-	45.8	0.56	43.3	5.79	1.18	0.06	0.08	0.73	0.16	0.03	1.65	99.4	35	20	160	70	8	15
186Ai	2	-	54.5	0.04	41.9	0.84	0.07	b.d.	0.13	0.71	0.25	0.10	1.43	99.9	36	21	150	7	b.d.	6
186Aii	1	1.5	30.8	1.86	37.7	19.7	4.50	0.32	0.40	0.73	0.33	0.23	4.05	100.7	34	33	140	209	10	59
186Aiii	1	3	35.2	1.74	36.7	15.3	2.77	0.17	0.27	2.1	1.10	0.05	4.25	99.7	96	115	480	228	10	45
186Aiv	1	6	37.7	1.44	35.4	12.2	2.33	0.11	0.46	3.28	2.04	0.04	5.25	100.3	145	215	690	196	8	43
186Av	1	9	38.3	1.35	33.9	11.3	2.66	0.09	0.54	3.76	2.50	0.09	5.66	100.2	167	262	800	184	8	41
186B	0	-	54.9	0.93	24.9	9.28	1.04	0.16	0.42	3.36	1.46	0.09	3.41	100	149	151	b.d.	123	14	25
186D	0	-	55.5	0.93	25.2	8.93	1.22	0.17	0.48	2.59	1.26	0.11	3.42	99.8	120	158	650	116	16	28
188A1	0	-	53.5	1.12	25.1	9.53	2.06	0.14	0.31	2.85	1.79	0.12	3.64	100.1	119	156	510	152	15	23
188A2	0	-	52.0	1.10	26.5	9.00	1.84	0.13	0.35	3.04	2.00	0.09	3.84	99.9	127	175	550	164	14	23
189A	1	-	40.2	1.48	32.7	15.5	2.96	0.32	0.14	0.79	0.48	0.07	4.11	98.8	38	33	140	224	22	48
192B	1	-	32.1	1.71	38.2	16.9	1.86	0.60	0.91	1.89	1.58	0.11	4.28	100.2	86	175	460	214	32	43
194A	1	-	33.4	1.63	40.4	14.5	0.98	0.28	1.63	1.92	1.75	0.06	3.77	100.4	85	232	450	208	38	39
195A	1	-	36.1	1.30	41.2	12.3	1.91	0.25	0.35	2.59	0.78	0.16	3.55	100.5	125	78	580	151	17	36
195B	1	-	35.6	1.30	47.2	11.6	1.76	0.08	0.54	0.33	0.20	0.40	2.07	101.1	16	28	50	112	17	111
198A	0	-	51.3	1.23	26.4	9.72	2.31	0.20	0.79	2.23	1.73	0.23	4.24	100.4	83	183	560	188	19	14
199A	0	-	49.7	1.08	30.4	9.06	1.28	0.13	0.60	3.18	1.10	0.14	3.88	100.6	133	159	830	134	11	30
199B	0	-	53.6	0.98	24.9	9.72	1.28	0.08	0.31	3.76	1.65	0.13	3.49	100.0	169	172	680	130	17	20
202A	0	-	52.3	1.00	27.2	9.99	1.31	0.09	0.59	2.95	1.33	0.18	3.41	100.4	140	147	630	118	17	26
202C	0	-	54.7	0.95	25.5	9.32	1.91	0.27	0.44	2.48	1.29	0.13	3.56	100.6	111	135	600	122	11	18

[a] Rb, Sr, Ba, Zr, Nb, and Y concentrations are tabulated in ppm, all others are listed in weight percent. All Fe is Fe_2O_3. *LOI*: loss on ignition. *b.d.*: below detection.
[b] R.C. = Rock Codes: 0, unaltered precursor schist; 1, altered selvage near vein; 2, quartz-kyanite vein.
[c] JAB181A and JAB186A-E are geochemical traverses that extend across alteration selvages adjacent to quartz veins. X indicates the approximate distance along a geochemical traverses measured in centimeters measured relative to X = 0 cm at the center of the veins.
[d] *Total*: weight percent total including Rb, Sr, Ba, Zr, Nb, and Y summed as oxides.

Table 2: Selected trace elements (ppm)[a]

Sample	La	Ce	Pr	Nd	Sm	Eu	Gd	Tb	Dy	Ho	Er	Tm	Yb	Lu	Nb	Hf	Ta	Th	Cr	Ni	Y
165A2	6.3	14.7	1.89	6.2	1.3	0.30	1.09	0.22	1.63	0.38	1.30	0.23	1.6	0.32	16	5	1.6	13.3	0.02	79	8.5
165A3	7.7	16.1	2.06	7.1	1.4	0.28	1.18	0.23	1.43	0.31	1.07	0.19	1.4	0.25	19	4	1.7	10.2	0.02	64	7.4
171A	61.4	114	14.0	50.3	8.7	1.69	7.74	1.23	6.46	1.24	3.61	0.50	3.0	0.51	18	4	1.6	15.8	0.01	66	31.9
172A	4.0	7.3	0.94	3.5	0.9	0.16	1.00	0.18	1.43	0.33	1.08	0.17	1.2	0.31	17	4	1.5	12.5	0.02	64	7.3
175Ai	20.5	38.2	4.94	18.7	3.5	0.68	2.57	0.28	1.07	0.13	0.21	b.d.	0.2	b.d.	b.d	b.d.	b.d.	0.8	b.d.	7	2.4
175Aiii	25.7	50.3	6.47	23.1	4.6	1.02	4.77	0.92	5.96	1.28	3.70	0.55	3.6	0.52	23	5	1.6	14.6	0.02	68	32.8
176A1	285	456	56.2	209	36.5	7.19	34.2	4.77	21.7	3.68	8.85	1.19	7.2	1.04	15	5	1.1	9.5	0.02	162	93.8
176A2i	177	281	34.4	126	21.5	4.34	20.7	2.68	11.2	1.74	3.98	0.49	3.0	0.43	12	1	0.6	7.2	0.01	33	48.4
177A	81.2	181	24.0	84.3	15.2	2.74	11.4	1.94	10.8	2.21	6.54	0.93	6.3	0.94	98	9	7.3	37.7	0.04	56	57.2
180B	45.0	87.7	11.4	41.1	8.5	1.96	9.23	1.84	12.0	2.58	7.60	1.14	7.4	1.10	18	10	2.7	35.3	0.04	69	65.6
181Ai	17.0	32.8	3.95	13.7	2.3	0.43	1.73	0.22	0.93	0.16	0.41	b.d.	0.3	0.05	3	b.d.	b.d.	2.3	b.d.	b.d.	3.6
181Aii	193	347	42.7	153	26.8	5.31	24.6	3.17	13.6	2.08	4.95	0.63	3.9	0.57	15	3	0.9	11.4	0.02	44	53.6
181Aiii	123	226	28.4	100	17.8	3.60	15.9	2.27	10.7	1.89	4.90	0.69	4.2	0.62	23	5	1.5	18.6	0.02	82	48.2
181Aiv	99.4	192	23.8	83.2	15.0	2.91	13.0	1.97	10.1	1.76	4.62	0.64	4.1	0.64	23	6	1.4	24.5	0.03	100	44.8
181C	23.8	48.5	6.04	20.9	4.3	1.06	6.25	1.41	10.9	2.52	7.58	1.12	7.3	1.08	19	7	1.2	13.1	0.03	99	67.0
181D	19.6	39.0	4.85	17.8	3.8	0.94	5.32	1.26	9.17	2.17	6.63	0.98	6.4	0.93	20	8	1.1	18.4	0.04	94	56.1
181E	45.7	93.4	11.7	41.0	7.7	1.55	7.19	1.33	8.33	1.82	5.33	0.80	5.2	0.74	16	6	0.8	20.7	0.03	110	47.3
182A	26.7	50.4	6.38	23.0	4.9	1.13	6.1	1.30	9.17	2.08	6.40	0.94	5.8	0.87	17	6	1.2	14.7	0.03	42	57.3
183A	21.5	39.1	4.91	17.8	3.4	0.69	3.36	0.59	3.39	0.72	1.97	0.29	2.0	0.28	8	2	b.d.	5.0	0.01	38	17.7
186Ai	77.6	154	19.3	69.2	11.2	1.98	7.49	0.80	2.46	0.28	0.57	b.d.	0.4	b.d.	b.d.	b.d.	b.d.	1.6	b.d.	14	6.4
186Aii	56.6	101	12.9	48.7	8.5	1.74	9.37	1.67	11.3	2.64	7.46	1.10	7.0	1.03	11	6	b.d.	19.2	0.03	126	66.3
186Aiii	25.3	49.5	6.59	25.3	4.7	1.04	5.47	1.11	8.33	1.80	5.51	0.76	5.0	0.72	11	7	1.0	21.9	0.03	87	46.8
186Aiv	47.8	93.8	11.9	46.4	8.8	1.76	8.16	1.39	8.77	1.97	5.46	0.80	5.1	0.75	9	6	0.7	21.3	0.03	77	47.5
186Av	79.0	150	18.7	72.6	13.1	2.51	11.3	1.64	8.98	1.75	4.53	0.66	4.1	0.63	8	5	0.6	20.9	0.02	85	42.4
186B	13.6	27.1	3.51	12.8	2.8	0.65	3.46	0.74	5.31	1.21	3.46	0.50	3.2	0.48	17	4	1.0	10.7	0.02	52	31.8
186D	85.3	154	18.3	64.8	11.2	2.18	9.76	1.43	7.02	1.24	3.43	0.46	2.9	0.40	17	3	1.0	14.8	0.02	55	30.3
188A1	42.5	74.9	9.54	33.6	6.4	1.27	5.71	0.91	5.04	1.02	3.36	0.54	3.9	0.57	17	5	1.3	14.7	0.02	60	25.3
188A2	37.0	59.2	7.30	25.8	4.8	1.02	4.87	0.79	4.55	0.97	3.16	0.53	3.4	0.53	16	6	1.3	16.9	0.01	56	25.9
189A	105	200	26.9	98.7	18.2	3.49	15.6	2.27	11.2	2.22	6.02	0.85	5.5	0.78	25	7	1.8	21.8	0.02	88	55.6
192B	35.4	67.0	8.38	30.6	5.9	1.28	6.36	1.26	8.47	1.86	5.48	0.84	5.1	0.76	35	7	2.4	23.8	0.03	73	47.7
194A	33.0	68.7	8.97	32.3	6.1	1.25	5.94	1.16	7.36	1.62	4.80	0.69	4.3	0.64	42	6	2.3	22.3	0.03	37	42.5
195A	51.2	91.9	11.2	40.1	7.5	1.52	7.47	1.28	7.71	1.56	4.70	0.68	4.2	0.63	20	5	1.4	15.8	0.02	62	41.5
195B	440	667	76.3	272	42.7	8.68	41.4	5.47	23.7	3.95	8.83	1.07	5.7	0.85	20	4	1.2	11.3	0.02	54	128
198A	37.8	84.0	11.1	38.7	7.0	1.33	5.00	0.74	3.47	0.68	1.92	0.30	2.1	0.33	22	6	1.2	18.1	0.02	63	14.7
199A	143	312	38.7	133	22.6	4.16	14.7	2.04	8.46	1.43	3.46	0.47	3.0	0.41	13	4	0.8	15.9	0.02	47	33.3
199B	8.2	15.4	1.96	7.3	1.6	0.41	2.11	0.46	3.62	0.82	2.50	0.36	2.5	0.36	19	4	1.1	12.4	0.02	68	22.0
202A	15.3	30.1	3.94	14.8	3.0	0.58	2.83	0.57	3.86	1.04	3.50	0.57	3.8	0.57	19	4	1.1	12.9	0.02	68	26.7
202C	11.7	23.2	3.04	10.9	2.2	0.43	2.25	0.49	3.43	0.83	2.44	0.36	2.6	0.37	12	4	1.0	12.8	0.02	76	20.7

[a]See Table 1 for sample rock type codes and distance along traverses for samples.

Table 3: Calculated time-integrated fluid fluxes[a]

Δm_{Al}[b]	ΔC_{Al} (moles/m$^3_{fluid}$)	Fluid-Rock Ratio (m$^3_{fluid}$/m$^2_{rock}$)	q_{TI}[c] for L=10 m	q_{TI} for L=10^2 m	q_{TI} for L=10^3 m
10^{-2}	9.3	$4.4\cdot10^2$	$4.4\cdot10^3$	$4.4\cdot10^4$	$4.4\cdot10^5$
$10^{-2.25}$	5.3	$7.8\cdot10^2$	$7.8\cdot10^3$	$7.8\cdot10^4$	$7.8\cdot10^5$
$10^{-2.5}$	3.0	$1.4\cdot10^3$	$1.4\cdot10^4$	$1.4\cdot10^5$	$1.4\cdot10^6$
$10^{-2.75}$	1.7	$2.5\cdot10^3$	$2.5\cdot10^4$	$2.5\cdot10^5$	$2.5\cdot10^6$
10^{-3}	0.9	$4.4\cdot10^3$	$4.4\cdot10^4$	$4.4\cdot10^5$	$4.4\cdot10^6$

[a]Values calculated for various length scales of Al geochemical front propagation at 1.0 GPa and 600°C.
[b] m_{Al}: molality of Al in supercritical H_2O fluid (moles Al/kg^3 solvent)
[c] Time-integrated fluid fluxes (q_{TI}) are in units of m$^3_{fluid}$/m$^2_{rock}$